To the Graduate Council:

I am submitting herewith a thesis written by Scott Michael Arwood entitled "An Energy Model for Rock Slope Stability Analysis." I have examined the final copy of this thesis for form and content and recommend that it be accepted in partial fulfillment of the requirements for the degree of Master of Science, with a major in Civil Engineering.

Matthew Mauldon, Major Professor

We have read this thesis
and recommend its acceptance:

Accepted for the Council:

Associate Vice Chancellor and
Dean of the Graduate School

AN ENERGY MODEL FOR ROCK SLOPE STABILITY ANALYSIS

A Thesis
Presented for the
Master of Science
Degree
The University of Tennessee, Knoxville

Scott Michael Arwood
August 1996

ACKNOWLEDGMENTS

This research program was supported by a contract from the Tennessee Department of Transportation. I would like to thank Bill Trolinger and Harry Moore at the Division of Materials and Tests for their support and participation. Harry Moore suggested the field study site and made recommendations for the computer program, all of which were much appreciated. I would like to thank my major professor, Dr. Matthew Mauldon, for his guidance and support on this project and in my graduate studies. I also greatly appreciate Dr. Eric Drumm and Dr. Chris Pionke for serving on my thesis committee and for their assistance.

ABSTRACT

Analyzing the stability of rock slopes involves predicting the sliding stability of blocks formed by planes of weakness within the rock mass. Plane and wedge sliding analyses, for which there are one and two sliding surfaces, respectively, have been widely used for the last thirty years. For plane and wedge slides, given certain assumptions, the distribution of normal forces on the contact planes is statically determinate. The resisting and driving forces may then be calculated by limiting equilibrium methods and the factor of safety determined directly. Certain geologic environments, however, especially those of folded rocks, produce potential failures which cannot be modeled as either plane or wedge slides. In these slopes the sliding of blocks may occur along non-planar surfaces. Standard rock stability analysis methods presently available are not adequate to treat these folded rock slopes. For this reason, a new energy model has been developed that can analyze the stability of a rock block with any number of contact planes or a curved contact surface. This research extends previous work by Mauldon and Ureta (1995, 1996) and Ureta (1994) and formulates the energy model in terms of stresses.

This model can analyze the stability of a prismatic rock block with any number of sliding surfaces or a cylindrical block with a curved surface. The factor of safety is evaluated as a function of the block geometry, loading conditions, and frictional resistance. The block is acted upon by an active resultant force $\boldsymbol{R}$ which is resolved to components $\boldsymbol{R}_N$ and $\boldsymbol{R}_T$, the normal and tangent to the sliding surface, respectively. The tangential component provides the disturbing force on the block that causes movement.

The normal component is equilibrated by normal reactions on the sliding surfaces. These normal reactions, multiplied by the coefficient of friction, provide the frictional resistance to movement. The distribution of these normal contact forces, however, is statically indeterminate. The energy based approach described in this thesis finds the distribution of normal contact forces corresponding to the minimum potential energy of the system. Once the contact forces have been determined, the frictional force may be found and the factor of safety calculated.

A computer program, *ROCKSLIP*, is also presented to implement the model. The program is demonstrated on a case study slope in Carter County, Tennessee. This slope is an area of a past failure in cylindrically folded shale. Results indicate that this failure could have been predicted with the model and computer program. The results also show that treating this failure as a wedge with two sliding surfaces greatly overestimates the factor of safety, possibly leading to an unsafe design.

TABLE OF CONTENTS

CHAPTER 1: BACKGROUND AND PURPOSE 1

CHAPTER 2: LIMITING EQUILIBRIUM METHODS 5

Introduction 5

Plane Slides 5

Wedge Failures 6

CHAPTER 3: STABILITY OF PRISMATIC BLOCKS 11

Introduction 11

Normal Stiffness k_n 12

Model Formulation 13

Direction of Displacement 17

Distribution of Normal Stresses 19

CHAPTER 4: STABILITY OF CYLINDRICAL BLOCKS 23

Introduction 23

Curved Failure Surface 23

Special Cases 27

Circular Section 27

Partial Circles 30

Elliptical Section 31

CHAPTER 5: MODEL VALIDATION AND ANALYSIS 37

Introduction 37

Plane Slides 37

Wedge Failures 38

Prismatic Wedge versus a Tetrahedral Wedge 42

Truncated Prismatic Block 43

Accuracy of Prismatic Block Approximation 45

CHAPTER 6: COMPUTER PROGRAM IMPLEMENTATION 47

Introduction 47

Program Operation 47

1. Theory 47

2. Input 48

3. Loading an Image 49

4. Defining Failure Surface on the Image 50

5. Reading Coordinates from a Text File 51

6. Defining the Fold Axis Orientation 53

7. Input Friction Angle 55

8. Correcting Cross Section 55

CHAPTER 7: CASE STUDY 58

Introduction 58

Site Geology 58

Orientation Data Analysis 64

Analysis 66

Discussion 69

CHAPTER 8: CONCLUSIONS 73

REFERENCES 75

APPENDICES 80

APPENDIX A: Mathematical Algorithm of *ROCKSLIP* 81

Input Variables 81

Calculation Algorithms 81

APPENDIX B: Photographs and Field Data of the Biltmore Study Site 91

Field Data 94

VITA 97

LIST OF FIGURES

Figure 1 Two fold structures (a) a syncline, and (b) an anticline (Wilson, 1981). 3

Figure 2 Cylindrical block formed in folded rocks. 4

Figure 3 Cylindrical block idealized as a prismatic block. 4

Figure 4 Conditions for a plane slide. 7

Figure 5 Cross section of a plane slide. 7

Figure 6 Wedge failure in progress. 9

Figure 7 Section of wedge orthogonal to line of intersection. 9

Figure 8 Energy model of a prismatic rock block. 12

Figure 9 Normal stress-normal closure relation (after Barton et. al., 1985). 13

Figure 10 Section of the block in the XY plane. 14

Figure 11 Resultant force with its normal and tangential components. 14

Figure 12 Prismatic block section with normal contact stresses. 20

Figure 13 Cross section of a block with curved sliding surface. 24

Figure 14 Block with circular cross section. 27

Figure 15 Section shaped as partial circle. 30

Figure 16 Elliptical section with major semi-axis horizontal. 33

Figure 17 Elliptical section with major semi-axis vertical. 33

Figure 18 Graph of the normalized factor of safety ($K = \tan\phi \tan\delta$) versus the aspect ratio of the ellipse (log scale). 36

Figure 19 A two sided prismatic block and its true cross section. 40

Figure 20 (a) tetrahedral wedge and (b) one of its contact sides. 43

Figure 21 A truncated prismatic block and its cross section 44

Figure 22 Normalized factors of safety (K=tanϕ tanδ) of a circular block idealized as a prismatic block with m planes. 46

Figure 23 Opening window showing an image being loaded. 49

Figure 24 The selected image is displayed. 50

Figure 25 The failure surface is defined by clicking on points. 51

Figure 26 Coordinate system used in the input of points. 52

Figure 27 Lower hemisphere projection of eight planes of a fold and multiple β-axes. 54

Figure 28 Lower hemisphere projection of the normal vectors of eight fold planes used to determine the π-axis. 54

Figure 29 Final results are displayed including factor of safety and sections. 56

Figure 30 Recalculation of the factor of safety for different friction angles. 57

Figure 31 Study site location in Carter County, Tennessee (Elizabethton and Keenburg Quadrangles, 1969.) 59

Figure 32 Geologic provinces of the Appalachians (Rodgers, 1970). 60

Figure 33 The major faults of East Tennessee, including Carter County (Thornbury, 1965). 62

Figure 34 Generalized Tennessee rock column (Wilson, 1981). 63

Figure 35 Lower hemisphere projection of the poles to the bedding. 65

Figure 36 Weighted contour plot of the poles. 65

Figure 37 The best fit great circle and the fold axis. 66

Figure 38 The failure surfaces, all with a fold axis plunge of 11° and a friction angle of 20°, used in the analysis of the Biltmore site with their factors of safety.. 67

Figure 39 Factors of safety for each analysis of the Biltmore site for a range of friction angles. 68

Figure 40 Three sided block with plane 2 horizontal used in the discussion.. 70

Figure 41 Graph of β as a function of the angles of planes 1 and 3. 72

Figure 42 Apparent and true sections on a slope face. 83

Figure 43 Coordinate axes used in the transformation of the apparent section. 84

Figure 44 The study site at Biltmore, TN. 92

Figure 45 The bedding planes can be seen to the right of the failure. 92

Figure 46 The folded bedding is shown by the quartzite cementation. 93

Figure 47 This block shows the thin bedding and perpendicular cleavage. 93

Figure 48 The location of orientations measured at the Biltmore study site. 96

LIST OF SYMBOLS

A	=	an index set
c	=	cohesion on a surface
ds	=	incremental arc length
F_R	=	total frictional resisting force per unit length
FS	=	factor of safety against sliding
h	=	horizontal semi - axis of an ellipse
k_n	=	joint normal stiffness
L_i	=	length of surface i in XY plane
n_i	=	unit normal to surface i
P	=	perimeter of an ellipse
R	=	resultant force acting upon a rock block
R_N	=	component of R normal to the line of intersection
R_T	=	component of R tangent to the line of intersection
r	=	radius
S	=	surface length in the XY plane
u	=	displacement of the block
V	=	total potential energy
V_i	=	elastic potential energy of surface i
v	=	vertical semi - axis of an ellipse
W	=	weight

W_r = work done by the active forces on the block

α = dip angle

γ = unit weight

Δv = joint closure

δ = angle between the line of intersection and R

θ_i = angle between the normal to surface i and the positive X axis

θ_r = angle between R_N and the positive X axis

θ_u = angle of the displacement from the positive X axis

σ_i = normal stress on surface i

τ_i = stress due to friction on surface i

ϕ = angle of friction

CHAPTER 1: BACKGROUND AND PURPOSE

Determination of the stability of a rock slope involves predicting the behavior of a discontinuous rock mass where failure surfaces generally occur along preexisting discontinuities. These discontinuities may be bedding layers, which provide a plane of weakness at the interlayer contacts, or later occurring fractures. Early work in rock slope stability was performed by Londe et al. (1969,1970), John (1968), and Goodman (1976, 1970). Good references on current methodologies include Hoek and Bray (1981) and Turner and Schuster (1996). Many different mathematical and geometric techniques have been proposed, but only plane sliding and wedge sliding analyses have been widely used for the last thirty years. These two classic methods are based on limiting equilibrium and are usually evaluated with graphical methods, such as stereographic projection, or with computer programs. These methods assume that all shear stresses in the contact plane(s) directly oppose motion. This makes the distribution of normal forces on the contact planes statically determinate, given that there is one or two contact planes. The resisting and driving forces may therefore be calculated from the block weight, frictional forces, water forces, and other support forces. Then the factor of safety may be determined directly as the ratio of the resisting force over the disturbing force.

Certain geologic environments, however, produce blocks which cannot be modeled accurately as wedge or plane slides and cannot be evaluated with the methods discussed above. An example is a block formed by cylindrically folded sedimentary rocks. The sediments were initially deposited in horizontal bedding layers. In the millions of years

since, the rocks have been compressed horizontally by tectonic movement. This compression folded the depositional layers into ridges and valleys. As shown in Figure 1, the folds form synclines and anticlines, with synclines being concave upward and the anticlines concave downward. If the layers are folded and tilted, but not twisted, the normals to the bedding surfaces will remain coplanar and the folding is termed cylindrical (Ramsay and Huber, 1987). When these rocks are folded the interlayer contacts are weakened, analogous to bending a deck of cards, and interlayer slip may occur. When slopes are cut through these folded rocks, failures may occur along the contacts of these bedding layers. The sliding surface in such cases cannot be described as single plane or an intersection of two planes, but is a curved surface as in Figure 2. Studies have shown that if these blocks are idealized as a two plane wedge, as is commonly done in practice, the factor of safety may be overestimated by the use of the wedge model (Mauldon and Ureta, 1995, 1996; Ureta, 1994). A cylindrical block could be idealized as a prismatic block with multiple sliding planes, all with parallel lines of intersection, as shown Figure 3. The model for the stability of these prismatic blocks will be presented first and then extended to where the number of planes m approaches infinity. A local coordinate system, which will later be used in the model development, is also defined in Figures 2 and 3 with the Z axis parallel to the fold axis and X and Y in the plane orthogonal to the fold axis.

When the number of planes m is three or more the distribution of the normal forces on the sliding surfaces becomes statically indeterminate and cannot be determined by the equations of limiting equilibrium. The frictional resistance to sliding cannot be

calculated without these normal forces. The factor of safety is therefore indeterminate also, demonstrating the need for a new model that can assess the stability of these prismatic blocks and can work directly with a curved sliding surface.

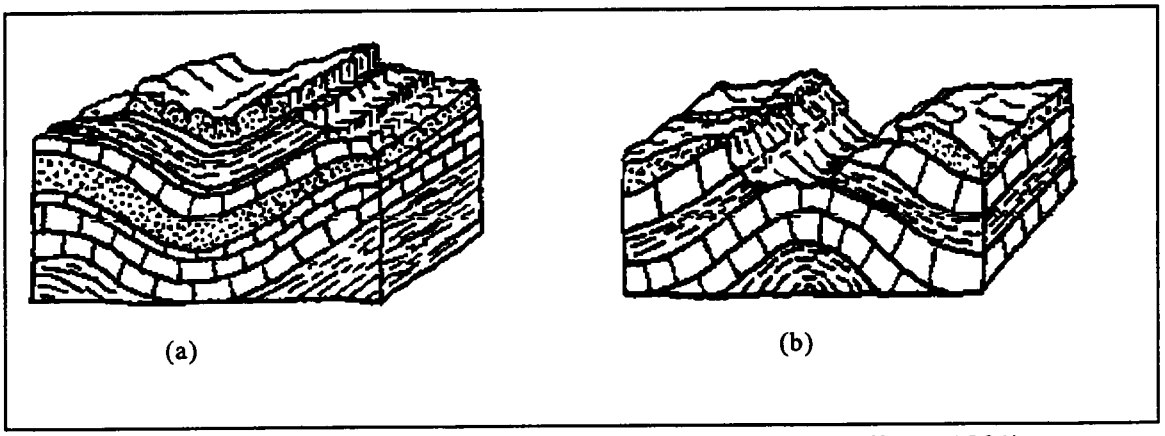


Figure 1 Two fold structures (a) a syncline, and (b) an anticline (Wilson, 1981).

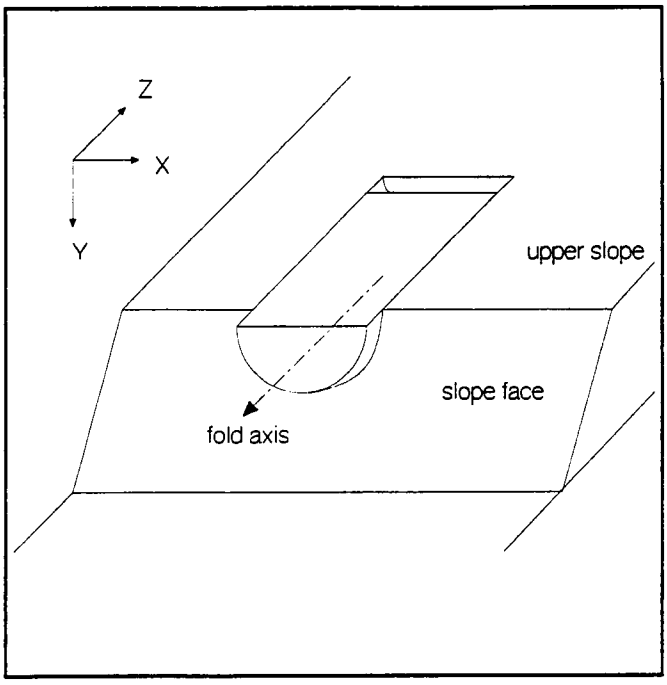


Figure 2 Cylindrical block formed in folded rocks.

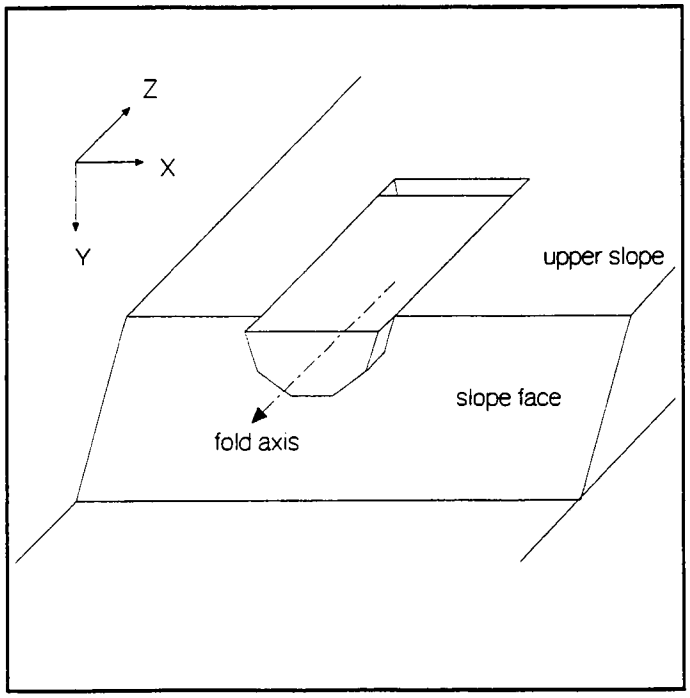


Figure 3 Cylindrical block idealized as a prismatic block.

CHAPTER 2: LIMITING EQUILIBRIUM METHODS

Introduction

As mentioned earlier, there are two commonly used limiting equilibrium methods in rock slope stability analysis, plane and wedge sliding models. In this chapter the two models are derived in their simplest forms, without water forces or cohesion. Both of these formulations are made possible by the assumption that the frictional forces directly oppose motion only and disappear in the plane orthogonal to the sliding direction.

Here, and throughout this thesis, geology and engineering geology terminology is used to describe the orientations of lines and planes. A line may be described by its plunge and trend. Plunge is defined as the angle between horizontal and the line, measured in the vertical plane. Trend is the compass direction of the horizontal projection of the downward end of the line, and in this thesis it will be given in degrees azimuth (clockwise from north). The orientation of a plane may be given by its dip and dip direction. The dip vector is a vector pointed down slope on the plane, perpendicular to a horizontal line (the strike line) on the plane. The angle between this vector and horizontal is referred to as the dip. The compass direction of the horizontal projection of the vector is the dip direction, again given in degrees azimuth.

Plane Slides

Plane slides may occur when one primary plane of weakness, or set of planes, is present in the rock mass. Development of plane failures requires that a number of

conditions are met. First, the strike of the discontinuity plane must be parallel or nearly parallel to the strike of the slope face. Second, the dip of the slope must be greater than the dip of the weak plane, causing the plane to daylight (become exposed) in the slope. Third, this exposed plane must dip at an angle greater than the angle of friction of the rock. If all these conditions are met, as in Figure 4, movement may occur. The factor of safety is expressed as the resisting force over the driving force, or with zero cohesion

$$FS = \frac{W\cos\alpha\tan\phi}{W\sin\alpha} = \frac{\tan\phi}{\tan\alpha} \qquad (1)$$

where W is the weight of the sliding mass, α is the dip of the weak plane, and ϕ is the angle of friction between the sliding block and the rock mass. A cross section cut perpendicular to the slope face is shown in Figure 5.

As can be seen in Equation (1), if the dip of the weak plane α is greater than the friction angle ϕ the factor of safety will be less than one. This means that the disturbing forces are greater than the stabilizing forces and the slope is potentially unstable.

Wedge Failures

Wedge failures are produced by the intersection of two planes of weakness within the rock mass (Figures 6,7). These two planes may form a tetrahedral block which may have the potential for sliding if the line of intersection daylights in the free face of the slope, as shown in Figure 6. For failure to occur, the trend of the line of intersection must be

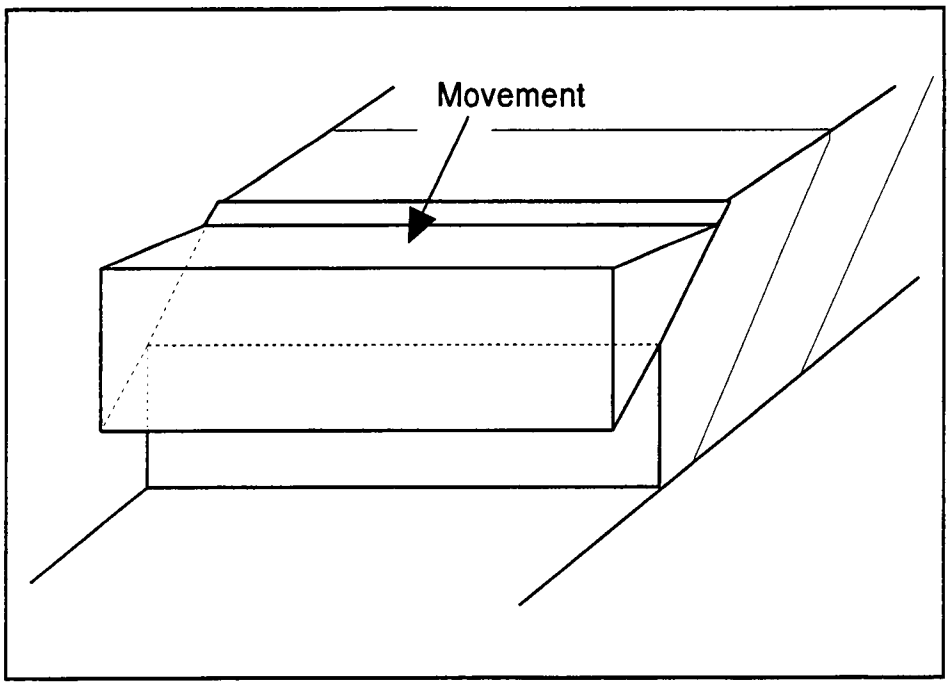


Figure 4 Conditions for a plane slide.

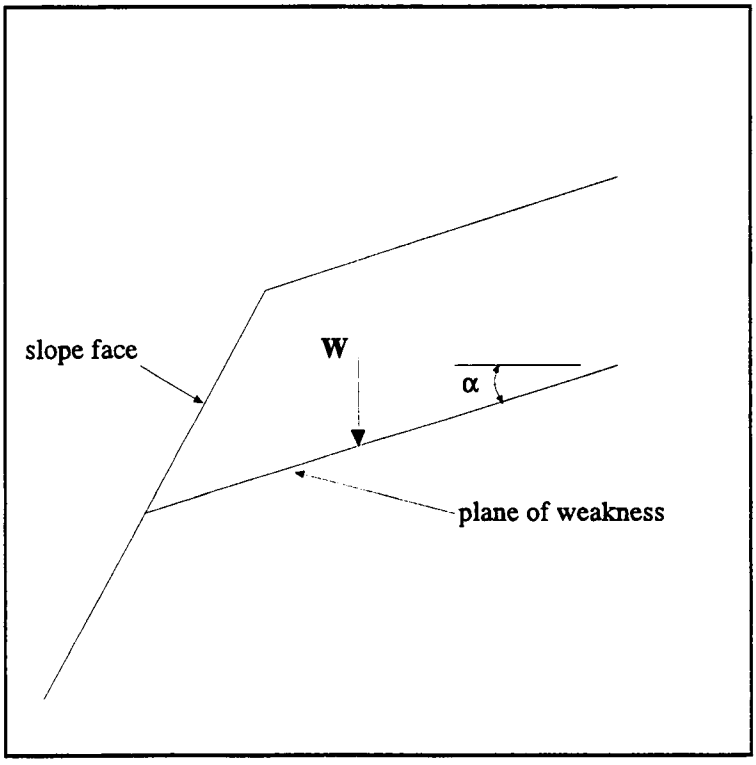


Figure 5 Cross section of a plane slide.

nearly parallel to the dip direction of the slope. Also, the dip of the slope must be greater than the plunge of the line of intersection, causing the line to daylight. This intersection line must plunge at an angle sufficiently steep such that the destabilizing forces exceed the shear resistance. Figure 7 shows a wedge viewed along the line of intersection with notation consistent with Hoek and Bray (1981). This is a statically determinate system and the forces can be calculated by limiting equilibrium. The factor of safety of a wedge with a friction angle of ϕ and zero cohesion is given by

$$FS = \frac{(R_A + R_B)\tan\phi}{W \sin\psi_i} \qquad (2)$$

where R_A and R_B are the normal reactions on the wedge from planes A and B and ψ_i is the plunge of the line of intersection. Resolving the forces horizontally and vertically produces two equations,

$$R_A \sin(\beta - \tfrac{1}{2}\xi) = R_B \sin(\beta + \tfrac{1}{2}\xi) \qquad (3)$$

$$R_A \cos(\beta - \tfrac{1}{2}\xi) - R_B \cos(\beta - \tfrac{1}{2}\xi) = W \cos\psi_i \ . \qquad (4)$$

where β and ξ are the angles as shown. Solving for R_A and R_B and adding produces

$$R_A + R_B = \frac{W \cos\psi_i \sin\beta}{\sin\tfrac{1}{2}\xi} \ . \qquad (5)$$

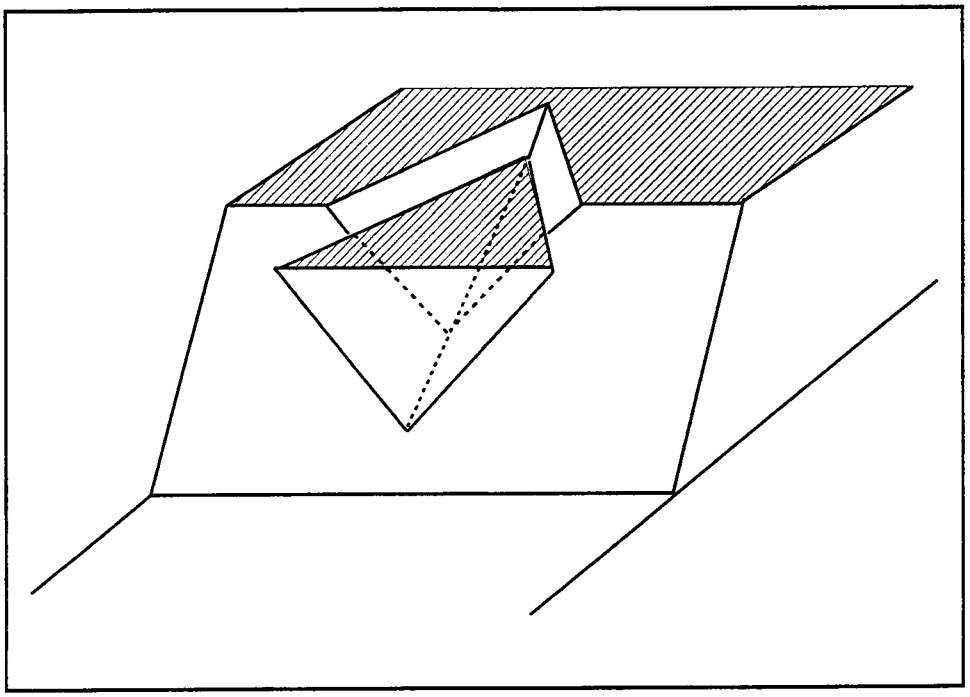


Figure 6 Wedge failure in progress.

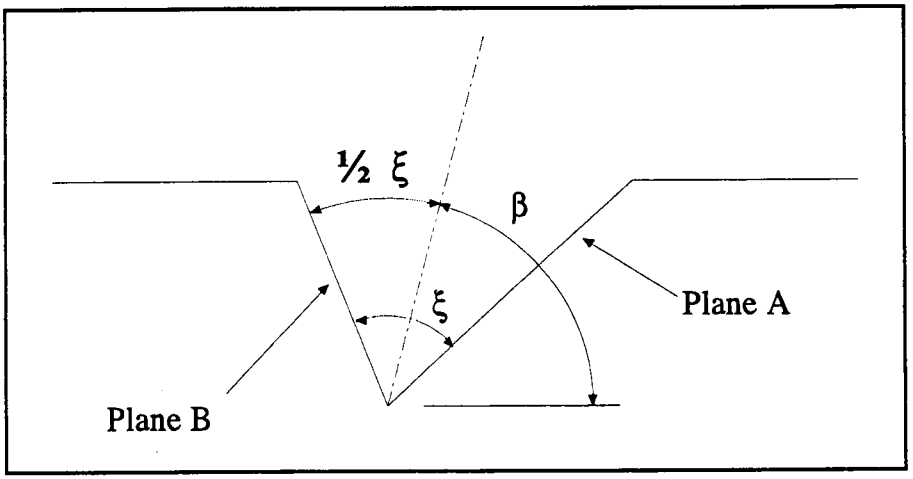


Figure 7 Section of wedge orthogonal to line of intersection.

With this the factor of safety for a wedge (Hoek and Bray, 1981) may be expressed as

$$FS = \frac{\sin\beta}{\sin\tfrac{1}{2}\xi}\frac{\tan\phi}{\tan\psi_i} \quad . \tag{6}$$

The angles relating to the geometry of the wedge may be found from a stereographic projection of the two planes.

CHAPTER 3: STABILITY OF PRISMATIC BLOCKS

Introduction

As stated earlier, when the number of planes of contact between a prismatic block and the rock mass is three or larger, the normal forces are statically indeterminate and the factor of safety cannot be determined by limiting equilibrium methods. In this chapter an energy model is introduced to evaluate the factor of safety against sliding of the prismatic block as a function of shear strength, cohesion, block geometry, and loading conditions. This method has been previously published in a similar form by Ureta (1994) and Mauldon and Ureta (1995, 1996). This formulation differs in the discussion of the stiffness of the rock contacts. In this thesis, each contact face the rock block is assumed to have a normal stiffness of k_n, whereas the previously published work employed a uniform spring stiffness constant for all contact surfaces. The block itself is assumed to be undeformable, deformation occurring only at the contact faces. The block is acted upon by an active resultant force $\boldsymbol{R}$, which includes self weight, and may include other forces. An important assumption is that the frictional shear stresses act parallel to the direction of sliding only (Hoek and Bray, 1981; Chan and Einstein, 1981). This is a standard assumption in the limiting equilibrium analyses presented previously. An elastic, conservative system is assumed to determine the distribution of normal forces that minimizes the potential energy of the system. These normal forces will then allow the stability to be determined. The coordinate system is the same as that defined in Figure 3.

Normal Stiffness k_n

The rock block itself is assumed to be undeformable, but elastic deformation occurs at the contacts between the block and the rock mass. The block-rock contacts are assumed to behave like linear springs with a joint normal stiffness (Brady and Brown, 1993; Franklin and Dusseault, 1989; Goodman, 1989) as in Figure 8.

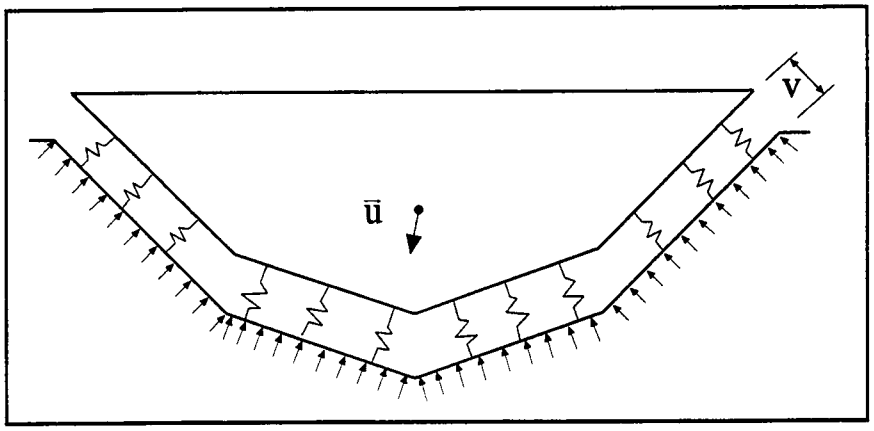


Figure 8 Energy model of a prismatic rock block.

Normal stiffness k_n is equal to the slope of a normal stress versus joint closure curve, i.e., $k_n = \sigma_n / \Delta v$, where σ_n and Δv are the normal stress and the joint closure, respectively. Most studies have shown that this curve will take a hyperbolic form (Goodman, 1989; Brady and Brown, 1993; Franklin and Dusseault, 1989) after a linear initial stiffness for low values of stress, as in Figure 9. Others have found a more linear relationship (Franklin and Dusseault, 1989). Normal stiffness has dimensions of force per unit volume, whereas the stiffness of a spring is given in force per length. It is often referred to in units of stress per unit length, such as gigaPascals per meter (Franklin and Dusseault, 1989). Generally, the stress-closure curve is linear during an initial stiffness

k_{ni} and then will become hyperbolic at large values of stress. Large amounts of closure occur initially, then the curve becomes asymptotic to the maximum possible closure v_m.

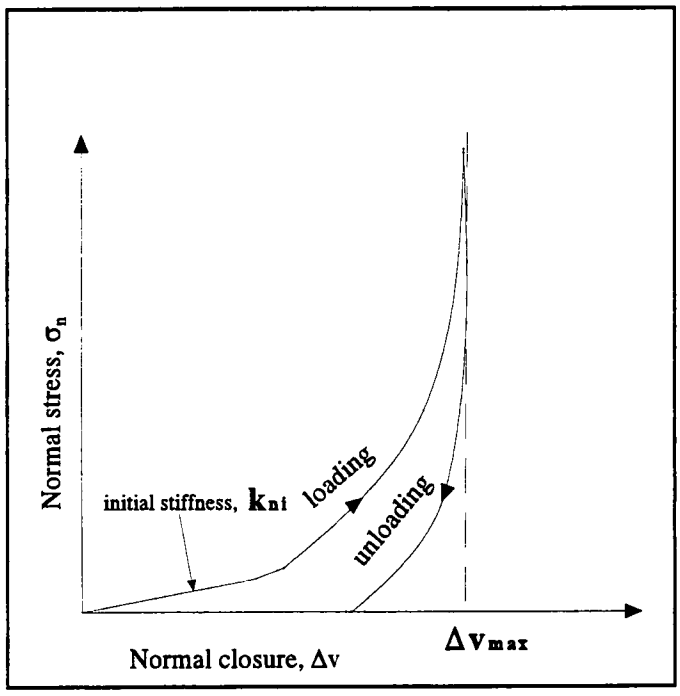


Figure 9 Normal stress-normal closure relation (after Barton et. al., 1985).

Model Formulation

Figure 10 shows a section of a prismatic block in the XY plane with the normal force $\boldsymbol{R}_n$ applied. Each discontinuity plane is defined by the angle, θ_i, between the positive X axis and the outward facing normal of that plane. The length of the ith discontinuity plane is denoted as L_i. R_N is the normal component of the resultant force as shown in Figure 11.

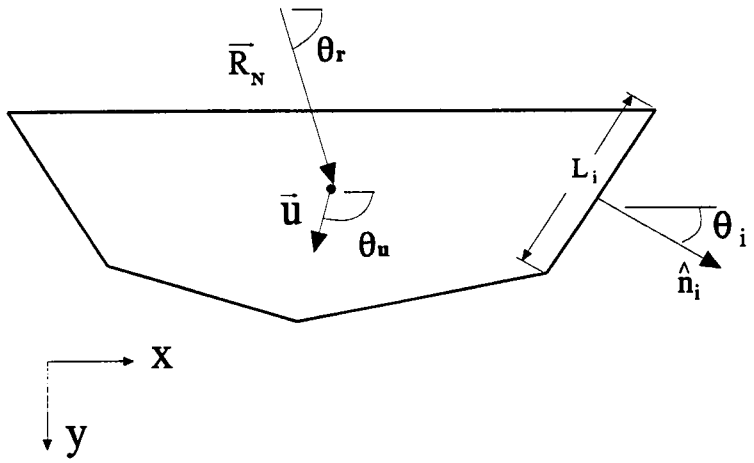


Figure 10 Section of the block in the XY plane.

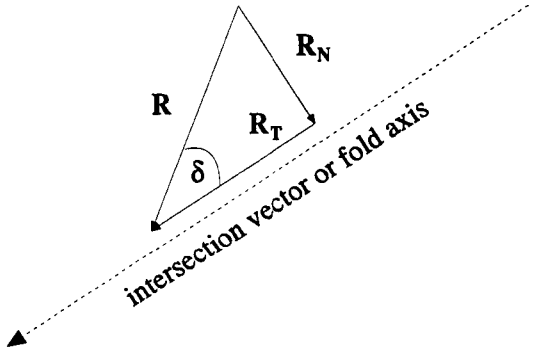


Figure 11 Resultant force with its normal and tangential components.

The "springs" at the contact faces have initially zero extension, thus establishing a datum for the gravitational potential energy. These springs are assumed to be perfectly linear elastic, as the stress is in the linear initial stiffness portion of Figure 9. Many hard and dense rocks are approximately linear elastic until cracks start to form at stress levels of approximately 60-70% of rupture (Franklin and Dusseault, 1989). If weight is the only force considered in the analysis, the stress levels at the contacts will be less than these values, and therefore linear elastic behavior can be assumed. In order to determine the distribution of contact forces it is assumed that the equilibrium position in the XY plane results from a small translational displacement of the block in the same plane (i.e., in the plane perpendicular to the potential sliding direction) under the action of the active forces. This small displacement is denoted by a vector $\vec{u}$ at an angle θ_u and with a magnitude u, as shown in Figure 10. Internal elastic strain energy is stored as a result of this displacement, i.e., the springs are compressed. The displacement $\vec{u}$ produces internal strain energy at the contact faces. The total potential energy of such a block comprising m discontinuity planes is the sum of the internal strain energy produced by the displacement and the potential of the external loads or

$$V=\sum_{i=1}^{m} V_i - W_r \tag{7}$$

where V_i, $i = 1,2, \ldots, m$ is the elastic potential energy associated with each discontinuity surface and W_r is the work done by the active forces acting on the block (Desai, 1979). The potential of the external load is lost through the work done by the load, hence the

negative sign. If self-weight is the only active force, then the work done by the active forces is the negative of the change in gravitational potential energy.

For an elastic spring, the elastic potential energy is defined as the integral of the force with respect to the displacement, which results in the quantity of one half the force multiplied by the deflection for a linear elastic spring. The force applied to each contact face is the normal stress multiplied by the contact area. Each plane has a length L_i in the XY plane, and since this is a prismatic block, the other dimension of the contact plane will be taken as a unit length in the Z (fold axis) direction. Therefore, the force applied will be $\sigma_i L_i$, but using the normal stiffness relationship discussed earlier, σ_i may be replaced by $k_n \Delta v_i$. Then the potential energy for the ith contact plane is

$$V_i = \tfrac{1}{2} k_n L_i \Delta v_i^2 \ . \tag{8}$$

The joint closure Δv_i may be expressed as the component of the displacement $\vec{u}$ in the normal direction of plane i, which may be found as the dot product of the displacement vector and the unit normal to each plane. Then for ith plane with its unit normal, $\hat{n}_i$, the elastic potential energy V_i is

$$V_i = \begin{cases} \tfrac{1}{2} k_n \ L_i \ (\hat{n}_i \cdot \vec{u})^2 & if\ (\hat{n}_i \cdot \vec{u}) > 0 \\ 0 & if\ (\hat{n}_i \cdot \vec{u}) \le 0 \end{cases} , \tag{9}$$

where the latter condition excludes tensile contact forces. It should be noted that the units are those of energy, force-length, because of a unit length within the equation. An index set A is defined for any displacement $\vec{u}$ as

$$A = A(\theta_u) = \{ i : \hat{n}_i \cdot \hat{u} > 0,\ i = 1,2,...,m \} \ . \qquad (10)$$

As can be seen, the index set A is a function of the angle of displacement and serves to include only those planes that remain in contact with the rock mass, ensuring no tension. Now Equation (7) can be expressed as

$$V = \sum_{i \in A} \tfrac{1}{2} k_n L_i \ (\hat{n}_i \cdot \vec{u})^2 - \vec{R}_N \cdot \vec{u} \qquad (11)$$

where the work W_r done by the active forces has been expressed as the dot product of the displacement vector and the component of the active resultant force perpendicular to the sliding direction. Expanding the dot products,

$$V = \sum_{i \in A} \tfrac{1}{2} k_n L_i \ u^2 \cos^2(\theta_u - \theta_i) - R_N u \cos(\theta_u - \theta_r) \qquad (12)$$

where R_N and u are magnitudes. In Equation (12) all angles are measured clockwise from the positive X axis, and are defined as in Figure 10.

Direction of Displacement

The system that has been described has two degrees of freedom, θ_u and u. The equilibrium condition is achieved when the total potential energy V of the system is stationary. Therefore there are two equilibrium requirements:

$$\frac{\partial V}{\partial \theta_u} = 0 \quad \& \quad \frac{\partial V}{\partial u} = 0 \ . \qquad (13)$$

Although the index set A changes with θ_u, the function V is piecewise continuous. Taking the partial derivatives,

$$\frac{\partial V}{\partial \theta_u} = \sum_{i \in A} (-k_n) L_i u^2 \cos(\theta_u - \theta_i) \sin(\theta_u - \theta_i) + R_N u \sin(\theta_u - \theta_r) = 0 \qquad (14)$$

and

$$\frac{\partial V}{\partial u} = \sum_{i \in A} k_n L_i u \cos^2(\theta_u - \theta_i) - R_N \cos(\theta_u - \theta_r) = 0 \ . \qquad (15)$$

If it is assumed for the present that the normal stiffness k_n is known, there are two equations, (14) and (15), and two unknowns, θ_u and u. The variables $u = u^*$ and $\theta_u = \theta_u^*$ denote the solutions. Solving (14) and (15) for u^*, two expressions are obtained:

$$u^* = \frac{R_N \sin(\theta_u^* - \theta_r)}{\sum_{i \in A} k_n L_i \cos(\theta_u^* - \theta_i) \sin(\theta_u^* - \theta_i)} \qquad (16)$$

and

$$u^* = \frac{R_N \cos(\theta_u^* - \theta_r)}{\sum_{i \in A} k_n L_i \cos^2(\theta_u^* - \theta_i)} \ . \qquad (17)$$

Equating the two above equations, the displacement u^* and the normal force R_N can be eliminated. Additionally, if the normal stiffness k_n is equal on all discontinuity surfaces it can be canceled to produce the simplified expression

$$\tan(\theta_u^*-\theta_r) = \frac{\sum_{i\in A} L_i \cos(\theta_u^*-\theta_i)\sin(\theta_u^*-\theta_i)}{\sum_{i\in A} L_i \cos^2(\theta_u^*-\theta_i)} \quad . \tag{18}$$

The angle θ_u^* which satisfies (18) gives the solution for the equilibrium condition for which the potential energy of the system is minimized. The angle of displacement is a function of the block geometry only, not the loading conditions. This angle is the only unknown in (18), but the form of this equation requires the use of a root solving routine to find θ_u^*.

Distribution of Normal Stresses

The prismatic block is acted upon by normal stresses on each of its contact planes due to the displacement in the *XY* plane (perpendicular to the sliding direction), as shown in Figure 12. The actual stresses have here been replaced by an equivalent mean surface stress. As stated earlier, the magnitude of the mean normal stress for each surface due to the small displacement $\vec{u}$ is computed as the normal stiffness multiplied by the magnitude of the displacement in the normal direction:

$$\sigma_i = k_n(\hat{n}_i \cdot \vec{u}^*) \tag{19}$$

or, expanding the dot product,

$$\sigma_i = k_n\, u^* \cos(\theta_u^*-\theta_i) \quad . \tag{20}$$

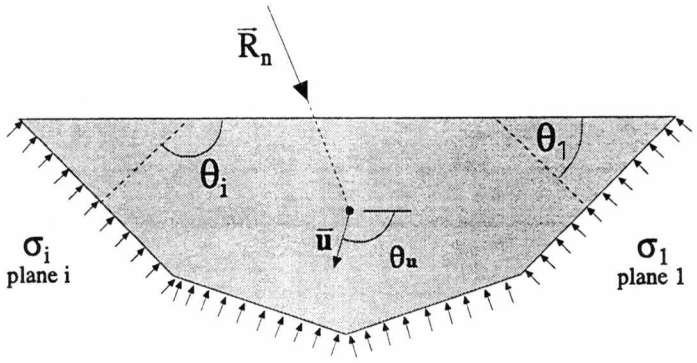


Figure 12 Prismatic block section with normal contact stresses.

The frictional strength may now be calculated for each plane as the coefficient of friction multiplied by the normal stress,

$$\tau_i = \tan\phi_i \, [k_n \, u^* \cos(\theta_u^* - \theta_i)] \tag{21}$$

where ϕ_i is the angle of friction on plane i. The total frictional resisting force, per unit length parallel to the fold axis (Z direction), is then the sum

$$F_R = \sum_{i=1}^{m} \tau_i \, L_i \ . \tag{22}$$

If the friction angle and the normal stiffness are assumed to be constant on all surfaces, the force can be expressed as

$$F_R = \tan\phi \, k_n \, u^* \sum_{i \in A} L_i \cos(\theta_u^* - \theta_i) \quad . \tag{23}$$

The magnitude of the displacement, u^*, can be obtained from Equation (17)

$$u^* = \frac{R_N \cos(\theta_u^* - \theta_r)}{k_n \sum_{i \in A} L_i \cos^2(\theta_u^* - \theta_i)} \tag{24}$$

assuming k_n to be constant. Substituting u^* into Equation (23), and canceling k_n,

$$F_R = R_N \tan\phi \cos(\theta_u^* - \theta_r) \frac{\sum_{i \in A} L_i \cos(\theta_u^* - \theta_i)}{\sum_{i \in A} L_i \cos^2(\theta_u^* - \theta_i)} \tag{25}$$

for the frictional resisting force. The driving force is denoted as R_T, the component of the active resultant force acting parallel to the fold axis. Therefore, the factor of safety can be expressed as the resisting force over the driving force as

$$FS = \frac{F_R}{R_T} \tag{26}$$

or substituting Equation (25) for F_R,

$$FS = \frac{R_N}{R_T} \tan\phi \cos(\theta_u^* - \theta_r) \frac{\sum_{i \in A} L_i \cos(\theta_u^* - \theta_i)}{\sum_{i \in A} L_i \cos^2(\theta_u^* - \theta_i)} \quad . \tag{27}$$

R_N and R_T may be replaced by (R sin δ) and (R cos δ), respectively, where the angle δ was defined as the angle between the fold axis and the direction of the resultant $\boldsymbol{R}$, as shown in Figure 11. For gravitational only loading, δ will be 90° minus the plunge of the fold axis (or intersection vector). Therefore, the magnitude R may be canceled in the factor of safety to yield

$$FS = \tan\delta \tan\phi \cos(\theta_u^* - \theta_r) \frac{\sum_{i \in A} L_i \cos(\theta_u^* - \theta_i)}{\sum_{i \in A} L_i \cos^2(\theta_u^* - \theta_i)} \quad . \tag{28}$$

Equation (28) gives the factor of safety against sliding for a prismatic block with m contact planes. If the friction angle ϕ varied among the different contact planes, then $\tan \phi_i$ would remain within the summation of the numerator of (28). Also, if the normal stiffness k_n varied, then k_{ni} would remain in each summation of (28). This final result is the same as previously published in Ureta (1994) and Mauldon and Ureta (1995, 1996). Note that the factor of safety does not depend on the magnitude of the resultant, only on the geometry, direction of displacement, and the friction angle. To calculate a factor of safety for a prismatic block the angle θ_u^* must first be calculated using Equation (18). With the geometric properties being known, the factor of safety may then be calculated from (28) using an appropriate friction angle.

CHAPTER 4: STABILITY OF CYLINDRICAL BLOCKS

Introduction

In the preceding formulation a cylindrical block with a curved sliding surface was idealized as a prismatic block with m rectangular sides. The number of sides used to approximate the curved sliding surface is chosen to accurately represent the curved section, where, as discussed in Chapter 5, the larger the number of sides, the better the approximation. Many actual rock blocks can be realistically modeled as prisms. However, in certain geologic environments, particularly those of folded rocks, the contact surface is in fact a smooth curve. This chapter presents a new method which extends the previously published work of Mauldon and Ureta (1995, 1996) to work with curved surfaces directly, dealing with stresses rather than forces.

Curved Failure Surface

Suppose that for $i = 1...m$ the discontinuity plane lengths L_i approach zero (or the number of discontinuity planes approaches infinity). In this case the discontinuity surface will approach a curved cylindrical shape, and the summations in the preceding equations can be replaced by integrals over the curved surface S, and the plane lengths with an incremental arc length of ds, as in Figure 13. Taking the equation for the angle of displacement (18), and replacing the summations and plane lengths results in

Since this equation has θ as the variable, S and ds must be expressed as a function of θ

$$\tan(\theta_u^* - \theta_r) = \frac{\int_S \cos(\theta_u^* - \theta)\sin(\theta_u^* - \theta)\ ds}{\int_S \cos^2(\theta_u^* - \theta)\ ds} \quad . \tag{29}$$

also. If the trace of the section is given by the parametric equations $x = x(\theta)$ and $y = y(\theta)$, then the incremental arc length is

$$ds = \sqrt{\left(\frac{dx}{d\theta}\right)^2 + \left(\frac{dy}{d\theta}\right)^2}\, d\theta \quad . \tag{30}$$

To simplify the following equations, the quantity $((dx/d\theta)^2 + (dy/d\theta)^2)^{1/2}$ will hereafter be symbolized as $\rho(\theta)$. Replacing ds and expressing the integral over the angle θ results in

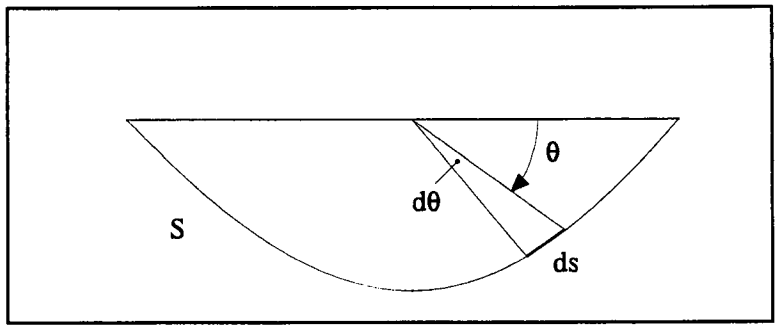


Figure 13 Cross section of a block with curved sliding surface.

$$\tan(\theta_u^* - \theta_r) = \frac{\int_\theta \cos(\theta_u^* - \theta)\sin(\theta_u^* - \theta)\ \rho(\theta)\, d\theta}{\int_\theta \cos^2(\theta_u^* - \theta)\ \rho(\theta)\, d\theta} \quad . \tag{31}$$

Using this relationship, the equation for the frictional resisting force, Equation (23), may now be expressed as

$$F_R = \tan\phi\, k_n u^* \int_\theta \cos(\theta_u^* - \theta)\ \rho(\theta)\, d\theta \quad . \tag{32}$$

Similarly, in Equation (17) the summation can be replaced by an integral and L_i replaced by incremental arc length,

$$u^* = \frac{R_N \cos(\theta_u^* - \theta_r)}{k_n \int_\theta \cos^2(\theta_u^* - \theta)\ \rho(\theta)\, d\theta} \quad . \tag{33}$$

Substituting Equation (33) into (32), the frictional resistance can be expressed as

$$F_R = R_N \tan\phi \cos(\theta_u^* - \theta_r) \frac{\int_\theta \cos(\theta_u^* - \theta)\ \rho(\theta)\, d\theta}{\int_\theta \cos^2(\theta_u^* - \theta)\ \rho(\theta)\, d\theta} \quad . \tag{34}$$

The factor of safety may be developed as previously defined as F_R over R_T to yield

$$FS = \tan\delta \tan\phi \cos(\theta_u^* - \theta_r) \frac{\int_\theta \cos(\theta_u^* - \theta)\ \rho(\theta)\, d\theta}{\int_\theta \cos^2(\theta_u^* - \theta)\ \rho(\theta)\, d\theta} \quad . \tag{35}$$

Again, an equation is produced which does not depend on the magnitude of the applied resultant force. If the contact surfaces exhibit any cohesion, the force on the discontinuity may also computed and added to the resisting force of the friction. The force will be the cohesion, c, multiplied by the surface area per unit length or

$$F_c = c \int_S ds = c \int_\theta \rho(\theta)\, d\theta \tag{36}$$

if the magnitude of the cohesion is constant. This term may be added to the frictional resisting force to obtain a total resisting force. Dividing both terms by the driving force R_T results in a factor of safety of

$$FS = \tan\delta \tan\phi \cos(\theta_u^* - \theta_r) \frac{\int_\theta \cos(\theta_u^* - \theta)\ \rho(\theta)\, d\theta}{\int_\theta \cos^2(\theta_u^* - \theta)\ \rho(\theta)\, d\theta} + \frac{c}{R_T} \int_\theta \rho(\theta)\, d\theta \quad . \tag{37}$$

When cohesion is added, the magnitude of the resultant must now be considered before a factor of safety may be found. The limits of integration are set to exclude areas of tension, as in the index set A. For a curved cylindrical surface, θ is limited to the closed

interval $(\theta_u^*-\pi/2, \theta_u^*+\pi/2)$, the semi-circle about the angle of displacement in the *XY* plane.

Special Cases

In the preceding equations integrals have been expressed in terms of a surface defined by $dx/d\theta$ and $dy/d\theta$. In the following sections some special cases are described where these integrals can be evaluated over a known surface shape.

Circular Section

A block with a circular cross section is shown in Figure 14. For such a circular section the parametric equations of the surface trace are $x = r \cos\theta$ and $y = r \sin\theta$, r being the radius, with $dx/d\theta = -r \sin\theta$ and $dy/d\theta = r \cos\theta$. Therefore, taking the square root of the sum of the squares, the quantity $\rho(\theta)$ will simplify to r.

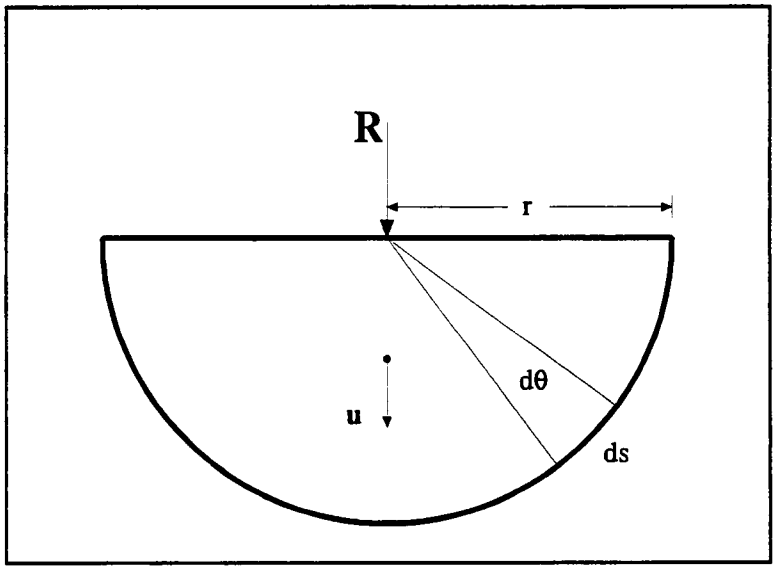


Figure 14 Block with circular cross section.

An incremental angle $d\theta$ will have an arc length of $rd\theta$. In the equation for the angle of displacement, (31), $\rho(\theta)$ is replaced by r, brought outside the integrals, and canceled. The limits of integration are set in accordance to the index set A, defined earlier to exclude tensile forces. The limits will be defined by the semi-circle about the angle of displacement θ_u^* to become

$$\tan(\theta_u^*-\theta_r) = \frac{\int_{\theta_u^*-\frac{\pi}{2}}^{\theta_u^*+\frac{\pi}{2}} \sin(\theta_u^*-\theta)\cos(\theta_u^*-\theta)\,d\theta}{\int_{\theta_u^*-\frac{\pi}{2}}^{\theta_u^*+\frac{\pi}{2}} \cos^2(\theta_u^*-\theta)\,d\theta} \quad . \tag{38}$$

The integral in the numerator of the above equation is equal to $-\frac{1}{2}\cos^2(\theta_u^*-\theta)$, and evaluating this at the limits of integration results in a value of zero. This shows, since $\tan(\theta_u^*-\theta_r) = 0$, that θ_u^* must equal θ_r. This is also true of any other section where the resultant force is parallel to a line of symmetry. In other words, the displacement will be in the direction of the resultant force. For gravity only loading, $\theta_r = \pi/2$. Noting that $\sin(\pi/2-\theta) = \cos\theta$, $\cos(\pi/2-\theta) = \sin\theta$, and $\cos(\theta_u^*-\theta_r) = \cos(0) = 1$, the final equation for the factor of safety for a circular block can be simplified to

$$FS = \tan\phi \tan\delta \frac{\int_0^{\pi} \sin\theta \, d\theta}{\int_0^{\pi} \sin^2\theta \, d\theta} + \frac{c}{R_T} \int_0^{\pi} r \, d\theta \ . \tag{39}$$

Equation (39) simplifies to

$$FS = \tan\phi \tan\delta \frac{4}{\pi} + \frac{c}{R_T} \pi r \tag{40}$$

with δ being defined as before. It should be noted that R is expressed as a force per unit length parallel to the fold axis and therefore the equation for the factor of safety is indeed dimensionless. As can be seen, the term in Equation (40) due to friction is scale independent, while the cohesion term is not. If weight is the only force being considered, R_T may be calculated as

$$R_T = R \cos\delta = \gamma \cdot \tfrac{1}{2} \pi r^2 \cos\delta \tag{41}$$

per unit width, with γ being the unit weight of the rock. Substituting this into the factor of safety will produce

$$FS = \tan\phi \tan\delta \frac{4}{\pi} + \frac{2}{r} \frac{c}{\gamma} \sec\delta \ . \tag{42}$$

This equation gives the factor of safety for a right circular cylinder based upon frictional resistance and cohesion. Note that the corresponding formula for the factor of safety of a

plane slide would be

$$FS = \tan\phi\tan\delta + \frac{1}{t}\frac{c}{\gamma}\sec\delta \qquad (43)$$

where t is the thickness of the sliding block. The factor of safety based upon the frictional resistance of the circular section is approximately one-third larger than the plane slide.

Partial Circles

A section shaped as a sector of a circle is shown in Figure 15. For this section the equations will be same as the circular section, except for the limits of integration. The limits are controlled not only by the direction of the force applied, but also by the geometry of the block.

The corresponding equations will be

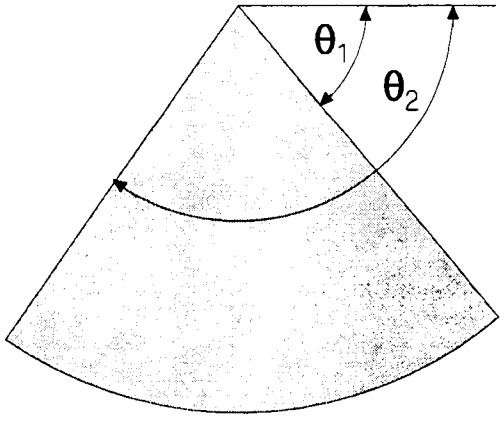


Figure 15 Section shaped as partial circle.

$$\tan(\theta_u^*-\theta_r) = \frac{\int_\alpha^\beta \sin(\theta_u^*-\theta)\cos(\theta_u^*-\theta)\,d\theta}{\int_\alpha^\beta \cos^2(\theta_u^*-\theta)\,d\theta} \tag{44}$$

and the factor of safety is

$$FS = \tan\phi\tan\delta\cos(\theta_u^*-\theta_r)\frac{\int_\alpha^\beta \cos(\theta_u^*-\theta)\,d\theta}{\int_\alpha^\beta \cos^2(\theta_u^*-\theta)\,d\theta} + \frac{cr}{R_T}\int_\alpha^\beta d\theta \ . \tag{45}$$

The angles α and β are defined by the direction of the force applied and the geometry of the partial circle as

$$\alpha=\max\left\{(\theta_u^* - \tfrac{\pi}{2}),\ \theta_1\right\} \qquad \beta=\min\left\{(\theta_u^* + \tfrac{\pi}{2}),\ \theta_2\right\} \ . \tag{46}$$

Unlike the circular section the partial circle will most likely not be symmetrical with respect to ***R***, and θ_u^* will not equal θ_r. Here θ_u^* must be calculated in order to find the factor of safety, whereas in a symmetrical section it did not.

Elliptical Section

In an elliptical section the displacement will also be in the direction of the resultant force, making θ_u^* equal to θ_r, if the ellipse is symmetric with respect to the direction of the force. This will cancel the term cos $(\theta_u^*-\theta_r)$ in the factor of safety equation as in the circular section. Thus the factor of safety for an ellipse is

$$FS = \tan\phi \tan\delta \frac{\int_{\theta} \cos(\theta_u^* - \theta)\, \rho(\theta)\, d\theta}{\int_{\theta} \cos^2(\theta_u^* - \theta)\, \rho(\theta)\, d\theta} + \frac{c}{R_T} \int_{\theta} \rho(\theta)\, d\theta \quad . \tag{47}$$

Also, if the assumption is made that the resultant force is vertical, the limits of integration are from 0 to π and $\theta_u^* = \pi/2$. An elliptical section may have the major semi-axis horizontal or the major semi-axis vertical as shown in Figures 16 and 17.

The horizontal semi-axis shall be referred to as h and the vertical semi-axis as v in this analysis. The incremental arc length can be found using the distance formula as $(ds)^2 = (dx)^2 + (dy)^2$. Using the parametric equations for an ellipse, $x = h\cos\psi$ and $y = v\sin\psi$ (see Figures 16 and 17), the derivatives are $dx = -h\sin\psi\, d\psi$ and $dy = v\cos\psi\, d\psi$, which results in

$$ds = \sqrt{h^2\sin^2\psi + v^2\cos^2\psi}\, d\psi \quad . \tag{48}$$

In order to solve the equations, ds must be found in terms of θ not ψ. It can be observed that the slope of the incremental arc segment dx/dy is equal to $-\tan\theta$. Also, relating the parametric equations given above,

$$\frac{dy}{dx} = \frac{v\cos\psi\, d\psi}{-h\sin\psi\, d\psi} = -\frac{v}{h}\cot\psi \quad . \tag{49}$$

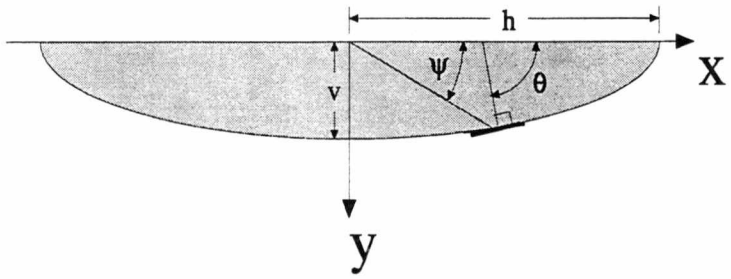


Figure 16 Elliptical section with major semi-axis horizontal.

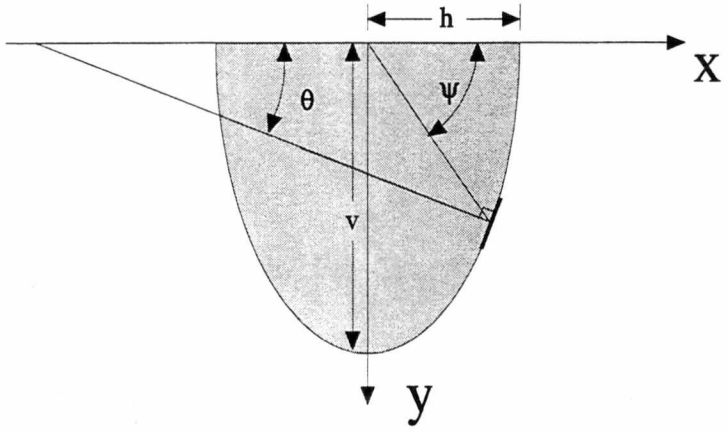


Figure 17 Elliptical section with major semi-axis vertical.

From these two relations it can be found that

$$\tan\theta = \frac{h}{v}\tan\psi \quad . \tag{50}$$

Using this relationship and trigonometric substitution, the incremental length *ds* may be expressed as

$$ds = \frac{hv}{\sqrt{h^2\cos^2\theta + v^2\sin^2\theta}}\, d\psi \ . \qquad (51)$$

In the equation above $d\psi$ must also be expressed in terms of θ. Differentiating (50) with respect to ψ and solving for $d\theta/d\psi$ leads to

$$\frac{d\theta}{d\psi} = \frac{v}{h}\sin^2\theta + \frac{h}{v}\cos^2\theta \ . \qquad (52)$$

Substituting the above expression for $d\psi$ in (51) and simplifying yields

$$ds = \frac{h^2v^2}{(h^2\cos^2\theta + v^2\sin^2\theta)^{\frac{3}{2}}}\, d\theta \qquad (53)$$

which is equivalent to $\rho(\theta)d\theta$. To simplify the following equations, $\chi(\theta)$ will denote $(h^2\cos^2\theta + v^2\sin^2\theta)^{3/2}$. Substituting (53) for $\rho(\theta)d\theta$ in Equation (47) and noting that $\cos(\pi/2-\theta)=\sin\theta$, the factor of safety is given by

$$FS = \tan\phi\tan\delta\frac{\int_0^{\pi}\frac{\sin\theta}{\chi(\theta)}\, d\theta}{\int_0^{\pi}\frac{\sin^2\theta}{\chi(\theta)}\, d\theta} + \frac{c}{R_T}\int_0^{\pi}\frac{h^2v^2}{\chi(\theta)}\, d\theta \ . \qquad (54)$$

In order to solve Equation (54) the integrals must be evaluated numerically. The integral in the second term of Equation (54) is equal to half the perimeter of the ellipse, from which

$$FS = \tan\phi\tan\delta \frac{\int_0^{\pi} \frac{\sin\theta}{\chi(\theta)}\, d\theta}{\int_0^{\pi} \frac{\sin^2\theta}{\chi(\theta)}\, d\theta} + \frac{c}{R_T}\left(\frac{1}{2}P\right) \quad . \tag{55}$$

The perimeter of the ellipse may be estimated (Spiegel, 1968) by the equation

$$P \approx 2\pi \sqrt{\tfrac{1}{2}(h^2+v^2)} \quad . \tag{56}$$

Also, for a unit thickness, R is given by the area of the ellipse multiplied by the unit weight, from which the component in the sliding direction is

$$R_T = \tfrac{1}{2}\pi h v \gamma \cos\delta \tag{57}$$

where γ is the unit weight of the rock. Using the above approximation, the factor of safety can now be expressed as

$$FS = \tan\phi\tan\delta \frac{\int_0^{\pi} \frac{\sin\theta}{\chi(\theta)}\, d\theta}{\int_0^{\pi} \frac{\sin^2\theta}{\chi(\theta)}\, d\theta} + \frac{2c\sqrt{\tfrac{1}{2}(h^2+v^2)}}{\gamma\, hv\cos\delta} \quad . \tag{58}$$

Note that if $h = v = r$ (i.e., the ellipse is in fact a circle) $\chi(\theta) = r^3$ and Equation (58) reduces to Equation (42). Equation (58) has been solved numerically, with zero cohesion, with the results graphically represented in Figure 18 as the normalized factor of safety for

various ellipse aspect ratios (v/h), where the normalizing factor is $K = \tan \phi \tan \delta$.

At $v/h = 1$ the ellipse becomes a circle and the quantity FS/K becomes $4/\pi$, which is indeed the factor given earlier for a circular section. This serves to verify the equations for the ellipses against the circular section equations. At $v/h = 0$ the ellipse becomes a horizontal planar surface and FS/K goes to 1, further verifying the model. As the ratio becomes large, the ellipse approaches a vertical planar surface and the factor of safety will increase without bound.

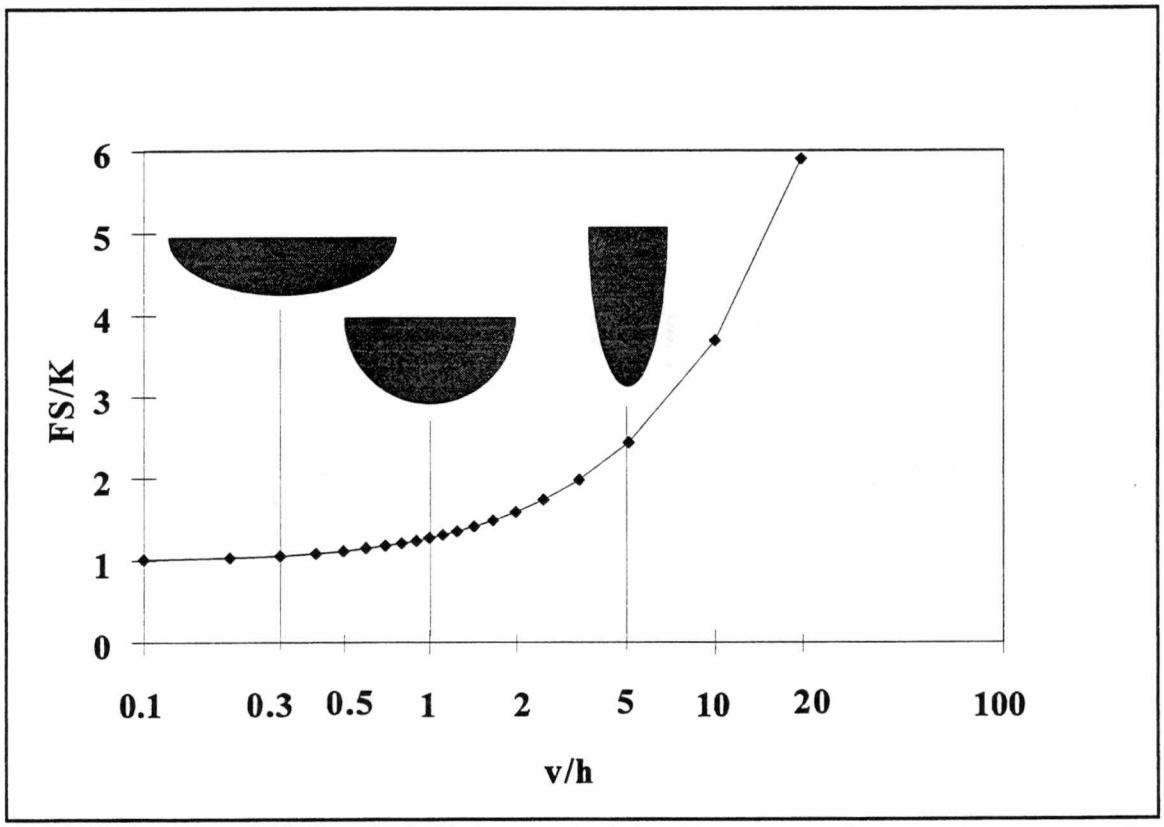


Figure 18 Graph of the normalized factor of safety (K= tanϕ tanδ) versus the aspect ratio of the ellipse (log scale).

CHAPTER 5: MODEL VALIDATION AND ANALYSIS

Introduction

In this chapter, the analytical model that has been presented is validated by comparing results obtained from the model with the results of limiting equilibrium methods. The methods discussed earlier are used to calculate a factor of safety for examples of plane and wedge slides. Then these factors of safety are compared to those obtained by using the energy model.

Plane Slides

Recall the equation derived previously for the factor of safety of a prismatic block (28):

$$FS = \tan\delta \tan\phi \cos(\theta_u^* - \theta_r) \frac{\sum_{i \in A} L_i \cos(\theta_u^* - \theta_i)}{\sum_{i \in A} L_i \cos^2(\theta_u^* - \theta_i)} \quad . \tag{59}$$

Recall that θ_u^* is the angle of the displacement vector in the XY plane (i.e., perpendicular to the sliding direction) with respect to the positive X axis. For a plane slide with gravity only loading, the sliding will be parallel to the Z axis (dip direction), making $\theta_u^* = 90°$. The angle θ_r was defined as the angle between the normal component of the resultant force and the positive X axis, and if weight is the only force considered this will also equal 90°. There is only one value of L_i, the width of the block, and it will cancel from the equation. The coordinate system is defined such that the normal to the sliding plane is parallel the Y axis, and hence θ_i is equal to 90°. Noting that the cosine of zero is unity,

Equation (59) reduces to

$$FS = \tan\delta \tan\phi \qquad (60)$$

which is equivalent to the limiting equilibrium equation developed in Chapter 2 (Equation (1)) with $\delta = 90° - \psi$.

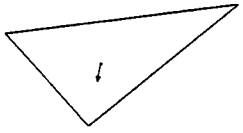
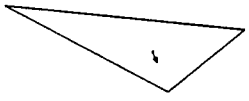
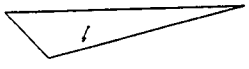
Wedge Failures

Three example wedges are defined by the dips and dip directions of their contact planes in Table 1. Weight is the only force being considered and the friction angle is taken to be 20°. The factor of safety was calculated for each wedge using the limiting equilibrium method of Hoek and Bray (1981) and the energy model developed here. Results and the true cross sections are shown in Table 2. As can be seen, the factors of safety are the same to at least five decimal places for each wedge, well beyond the practical limit for a factor of safety. They are essentially the same. The differences at this level may be explained by the rounding of numbers or by the approximation involved in Equation (18). If the lengths are changed the angle of displacement will change accordingly, but the factor of safety will not change. This is expected since the limiting equilibrium equation includes no terms for the lengths of the planes. The plane lengths in the energy equation for a two sided prismatic block can, in fact, be canceled as follows.

Table 1. Data for Sample Wedge Analysis

Wedge	Plane	Dip (degrees)	Dip Direction (degrees)	Length
1	1	40	235	1.5
	2	50	85	1
2	1	40	250	1
	2	30	100	2
3	1	20	255	3
	2	50	125	1

Table 2. Comparison of the Analysis Results of the Sample Wedges

Wedge	Limiting Equilibrium FS	Energy Model FS	θ_u*
 1	1.9495835	1.9495834	101.6°
 2	2.46303	2.46302	67.7°
 3	1.7993498	1.7993503	109.4°

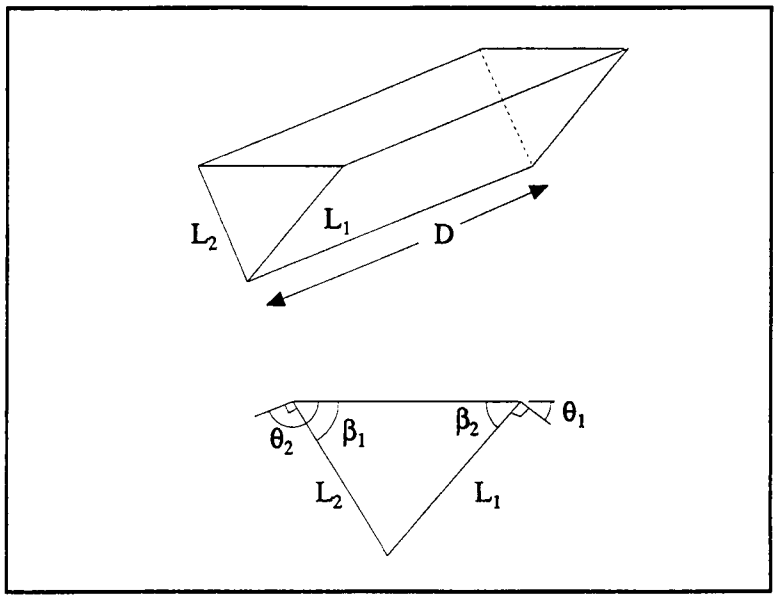


Figure 19 A two sided prismatic block and its true cross section.

Taking a two sided prismatic block as in Figure 19, the contact area of each side is $A_i=L_iD$. From this, the internal strain energy of side i is

$$V_i = \tfrac{1}{2}(k_n L_i D)\,(\hat{n}_i \cdot \vec{u})^2 \tag{61}$$

The total potential energy of this block is

$$V = \tfrac{1}{2} k_n D\left[L_1(\hat{n}_1 \cdot \vec{u})^2 + L_2(\hat{n}_2 \cdot \vec{u})^2\right] - \vec{R}_N \cdot \vec{u} \tag{62}$$

or, expanding the dot products,

$$V = \tfrac{1}{2} k_n D\, u^2\left[L_1 \cos^2(\theta_u^* - \theta_1) + L_2(\theta_u^* - \theta_2)^2\right] - R_N u \cos(\theta_u^* - \theta_r) \quad . \tag{63}$$

Taking the partial derivatives with respect to u and θ_u^* and setting these equal to zero produces the two equations for u,

$$u^* = \frac{R_N \cos(\theta_u^* - \theta_r)}{k_n D\left[L_1 \cos^2(\theta_u^* - \theta_1) + L_2 \cos^2(\theta_u^* - \theta_2)\right]} \tag{64}$$

and

$$u^* = \frac{R_N \sin(\theta_u^* - \theta_r)}{k_n D\left[L_1 \cos^2(\theta_u^* - \theta_1)\sin(\theta_u^* - \theta_1) + L_2 \cos^2(\theta_u^* - \theta_2)\sin(\theta_u^* - \theta_2)\right]} \quad . \tag{65}$$

Equating equations (64) and (65) eliminates R_N, k_n, D and produces the expression for the angle of displacement,

$$\tan(\theta_u^* - \theta_r) = \frac{L_1 \cos(\theta_u^* - \theta_1)\sin(\theta_u^* - \theta_1) + L_2 \cos(\theta_u^* - \theta_2)\sin(\theta_u^* - \theta_2)}{L_1 \cos^2(\theta_u^* - \theta_1) + L_2 \cos^2(\theta_u^* - \theta_2)} \quad . \tag{66}$$

For the cross section in Figure 19, the following relationship can be developed from the law of sines

$$\frac{L_1}{\sin\beta_1} = \frac{L_2}{\sin\beta_2} \quad \equiv \quad \frac{L_1}{L_2} = \frac{\sin\beta_1}{\sin\beta_2} \quad . \tag{67}$$

Noting the relationship between each θ and β and simplifying produces

$$\frac{L_1}{L_2} = \frac{\sin\left(\theta_2 - \frac{\pi}{2}\right)}{\sin\left(\frac{\pi}{2} - \theta_1\right)} = -\frac{\cos\theta_2}{\cos\theta_1} \quad . \tag{68}$$

If the numerator and the denominator of Equation (66) are multiplied by $1/L_2$, then the ratio L_1/L_2 can be replaced by the formulation of Equation (68) to produce

$$\tan(\theta_u^* - \theta_r) = \frac{\cos(\theta_2-\theta_u^*)\sin(\theta_2-\theta_u^*)\cos\theta_1 - \cos(\theta_1-\theta_u^*)\sin(\theta_1-\theta_u^*)\cos\theta_2}{\cos^2(\theta_1-\theta_u^*)\cos\theta_2 + \cos^2(\theta_2-\theta_u^*)\cos\theta_1} \qquad (69)$$

after simplification. Similarly, the factor of safety for a two sided prismatic block may be developed as

$$FS = \tan\phi \tan\delta \cos(\theta_u^* - \theta_r) \frac{\cos(\theta_1-\theta_u^*)\cos\theta_2 - \cos(\theta_2-\theta_u^*)\cos\theta_1}{\cos^2(\theta_1-\theta_u^*)\cos\theta_2 + \cos^2(\theta_2-\theta_u^*)\cos\theta_1}. \qquad (70)$$

Therefore, equations (69) and (70) show that the factor of safety for a two sided prismatic block does not depend upon the plane lengths, only on the angles.

Prismatic Wedge versus a Tetrahedral Wedge

Often wedges produced in nature are tetrahedral wedges rather than prismatic wedges. That is, the contact faces are triangular in shape rather than rectangular. An example of a tetrahedral wedge is shown in Figure 20. The contact area for each face is $A_i = \frac{1}{2} DH_i$. The true length for each side is the length in the plane orthogonal to line of intersection. Therefore, the true length L_i is equal to H_i and the contact area may be expressed $A_i = \frac{1}{2}DL_i$. Recall that for the prismatic block the contact area was twice that, $A_i = DL_i$.

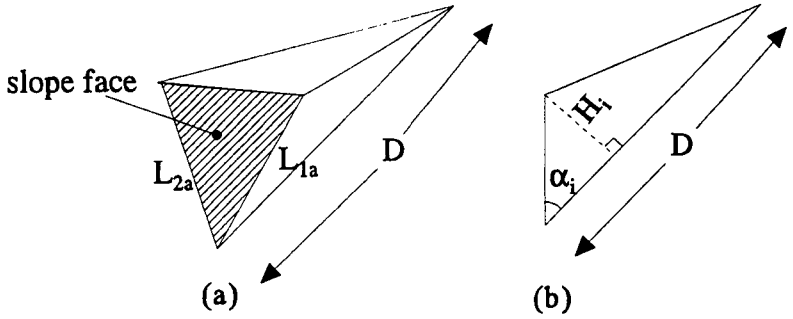


Figure 20 (a) tetrahedral wedge and (b) one of its contact sides.

When formulating the equations for the angle of displacement this ½ will cancel, just as the k_n and other quantities. The resulting equation is the same as for the prismatic wedge. Likewise, in formulating the factor of safety the ½ will cancel to produce an equation identical to the prismatic wedge.

Truncated Prismatic Block

Often there are blocks with three contact surfaces whose lines of intersection daylight in both the slope face and the upper slope, as in Figure 21. A five sided block is produced rather than a six sided block. In this case the constant of proportionality for plane 2 is different than that of planes 1 and 3, i.e., plane 2 is rectangular and planes 1 and 3 are triangular. The contact areas are $A_1 = \frac{1}{2} DH_1$, $A_2 = D L_2$, and $A_3 = \frac{1}{2} D H_3$. If the line of intersection and the dip direction of the slope are parallel, then the length H_i may be replaced by the true plane length L_i.

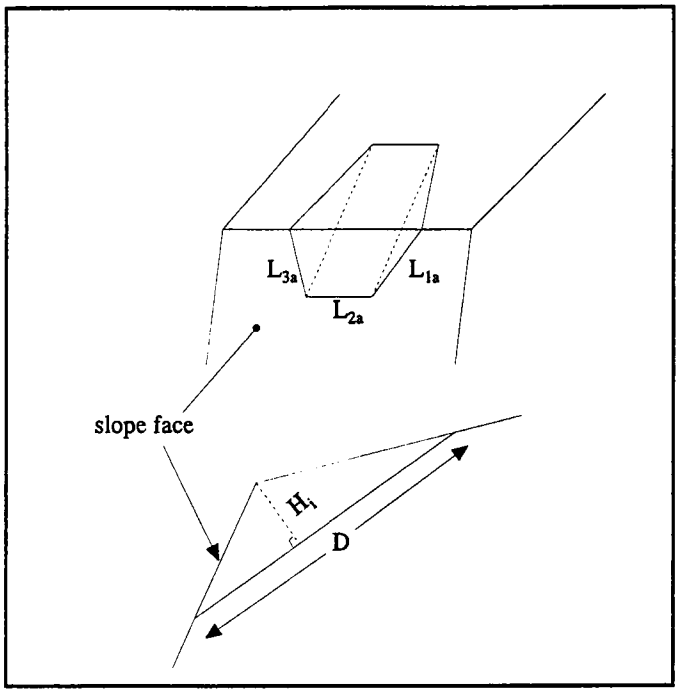


Figure 21 A truncated prismatic block and its cross section.

The strain energy for planes 1 and 3 are the same as the tetrahedral wedge, but for plane 2 it is

$$V_2 = \tfrac{1}{2}(k_n L_2 D)(\hat{n}_2 \cdot \vec{u})^2 \quad . \tag{71}$$

The total potential energy may be developed as before as the sum of the three strain energies and the potential of the external loads. The equation for the angle of displacement is derived in the usual manner to produce

$$\tan(\theta_u^* - \theta_r) = \frac{L_1 \cos(\theta_u^* - \theta_1)\sin(\theta_u^* - \theta_1) + 2L_2 \cos(\theta_u^* - \theta_2)\sin(\theta_u^* - \theta_2) + L_3 \cos(\theta_u^* - \theta_3)\sin(\theta_u^* - \theta_3)}{L_1 \cos^2(\theta_u^* - \theta_1) + 2L_2 \cos^2(\theta_u^* - \theta_2) + L_3 \cos^2(\theta_u^* - \theta_3)} \tag{72}$$

The factor of safety is also formulated in the usual manner to produce the equation

$$FS = \tan\phi \tan\delta \cos(\theta_u^* - \theta_r) \frac{L_1 \cos(\theta_u^* - \theta_1) + 2L_2 \cos(\theta_u^* - \theta_2) + L_3 \cos(\theta_u^* - \theta_3)}{L_1 \cos^2(\theta_u^* - \theta_1) + 2L_2 \cos^2(\theta_u^* - \theta_2) + L_3 \cos^2(\theta_u^* - \theta_3)} \qquad (73)$$

for this block. These two equations differ from those of a six sided prismatic block only by the factor of two in the plane 2 term.

Accuracy of Prismatic Block Approximation

When idealizing a curved surface as a prismatic surface, the question arises of how many planes are needed to make an acceptable estimate. To answer this, a circular block with the resultant force vector along the line of symmetry and no cohesion is analyzed. The exact factor of safety of such a block was developed earlier as

$$FS = \tan\phi \tan\delta \frac{4}{\pi} . \qquad (74)$$

The circular block is idealized as a prismatic block with two, four, eight, and sixteen sides with the results shown in Figure 22. The factors of safety have been normalized by dividing by K=tanϕ tanδ. As can be seen, the accuracy increases rapidly from two to four sides. The differences between the eight and sixteen sides and the circle are all less than one percent. This graph also shows that the factor of safety will be overestimated when using a wedge model to idealize a cylindrical block.

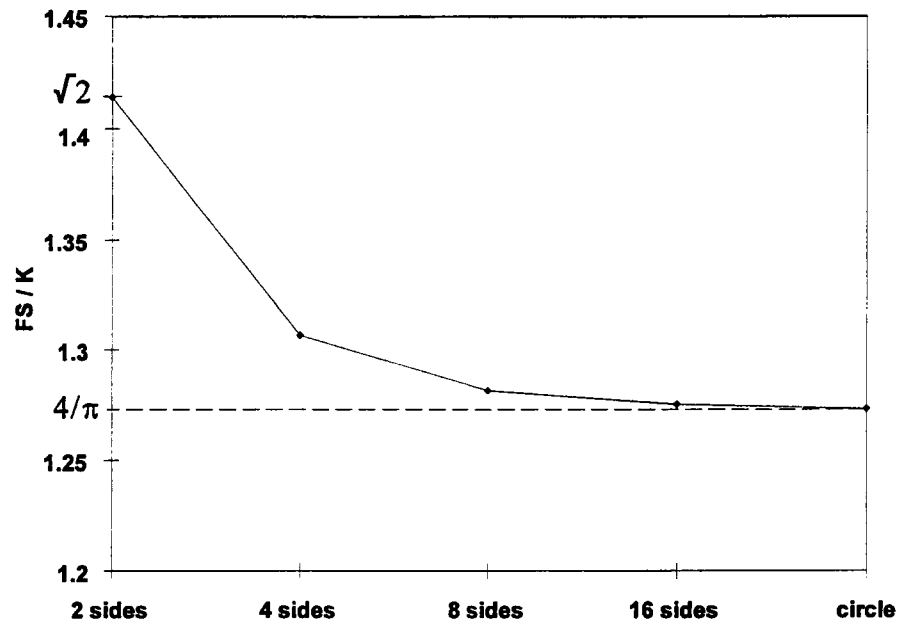


Figure 22 Normalized factors of safety (K= tanϕ tanδ) of circular block idealized as a prismatic block with *m* planes.

CHAPTER 6: COMPUTER PROGRAM IMPLEMENTATION

Introduction

The following is a user's guide to the computer program, given the name *ROCKSLIP*, developed to implement the energy model for rock slope stability. A more detailed description of the mathematical processes performed by the program may be found in Appendix A.

Calculation of the factor of safety using the analytical model can become quite laborious for all but the simplest of sections. To ease the amount of hand computations, a computer program named *ROCKSLIP* has been developed to implement the model for rock slope stability. The program is written in *Visual Basic* version 3.0, a programming language for the *Windows* environment. The completed program is indistinguishable from any other Windows program in setup and operation. Unlike earlier versions of BASIC, *ROCKSLIP* will run on a computer without the actual *Visual Basic* software loaded. *ROCKSLIP* will not run in a DOS environment.

Program Operation

1. ***Theory***

The factor of safety is calculated from the equation given for a prismatic block,

$$FS = \tan\delta \tan\phi \cos(\theta_u^* - \theta_r) \frac{\sum_{i \in A} L_i \cos(\theta_u^* - \theta_i)}{\sum_{i \in A} L_i \cos^2(\theta_u^* - \theta_i)} \qquad (75)$$

where θ_u^* is calculated from the expression

$$\tan(\theta_u^*-\theta_r) = \frac{\sum_{i\in A} L_i \cos(\theta_u^*-\theta_i)\sin(\theta_u^*-\theta_i)}{\sum_{i\in A} L_i \cos^2(\theta_u^*-\theta_i)} \quad . \tag{76}$$

The plane lengths L_i and their angles θ_i may be taken from the corrected image of the outcrop face. This version of *ROCKSLIP* assumes gravity loading and therefore the angle θ_r between the resultant force and the X axis is $\pi/2$. The friction angle ϕ and the angle δ will be discussed in Sections 6 and 7.

2. *Input*

The source of input for *ROCKSLIP* is intended to be a graphic image of the outcrop in question with the traces of bedding visible, or at a known location. The format of this image must be a *Windows* bitmap file (*.bmp). Examples of bitmaps are the files used for *Windows* wallpaper and files created by the *Windows Paintbrush* application. These images could be obtained in a number of different methods. A video of the outcrop could be taken and then images could be captured from that video using a video capturing card in the computer. This method is the most complicated and expensive, requiring a high quality video camera, a high performance computer, and a video capture card. A more likely method is to take photographs of the outcrop and have a photographic services company, such as Seattle Filmworks (see References), produce scanned images from the prints or slides, or the user could scan the images if a good quality scanner is available. This method would not require the purchase of additional hardware or equipment by the

user.

3. *Loading an Image*

Once *ROCKSLIP* is started, a window appears showing the drives and directories of the user's computer, allowing a bitmap to be loaded. Figure 23 shows a screenshot of this event. As shown in the figure, the user is also given the option of taking data points from a file, which is discussed in Section 5. After the bitmap is selected by doubling clicking or pressing the OK button, the image should appear as shown in Figure 24.

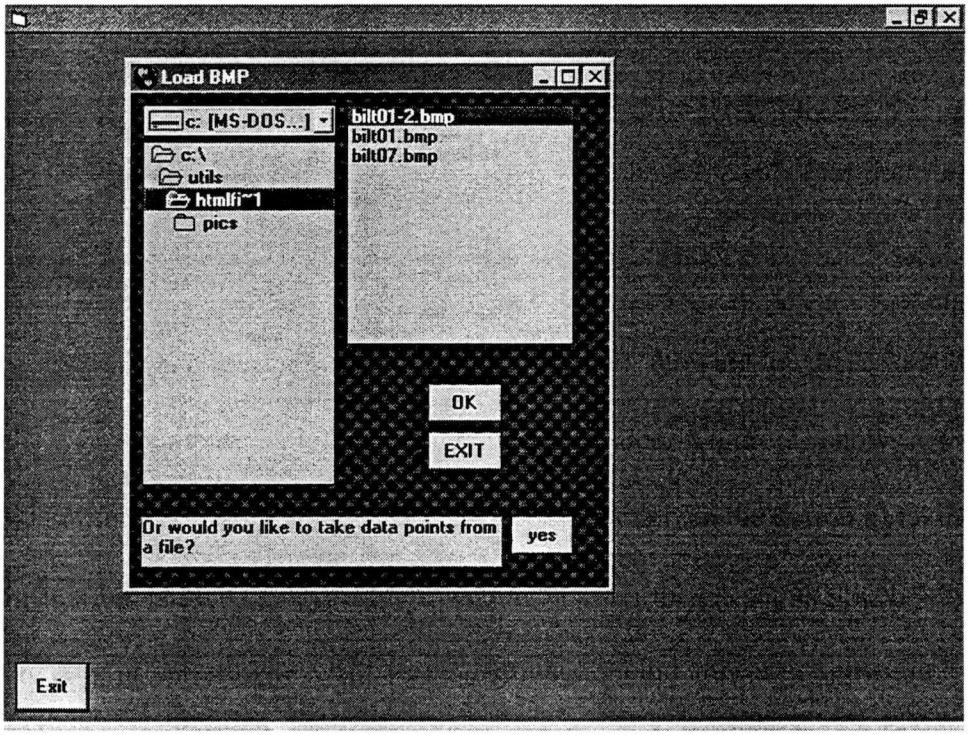


Figure 23 Opening window showing an image being loaded.

As shown in Figure 24, the bitmap has been loaded and appears in a window to the right of the screen. The smaller window to the left shows the position of the mouse pointer (which will appear as cross hairs) as it passes over the image.

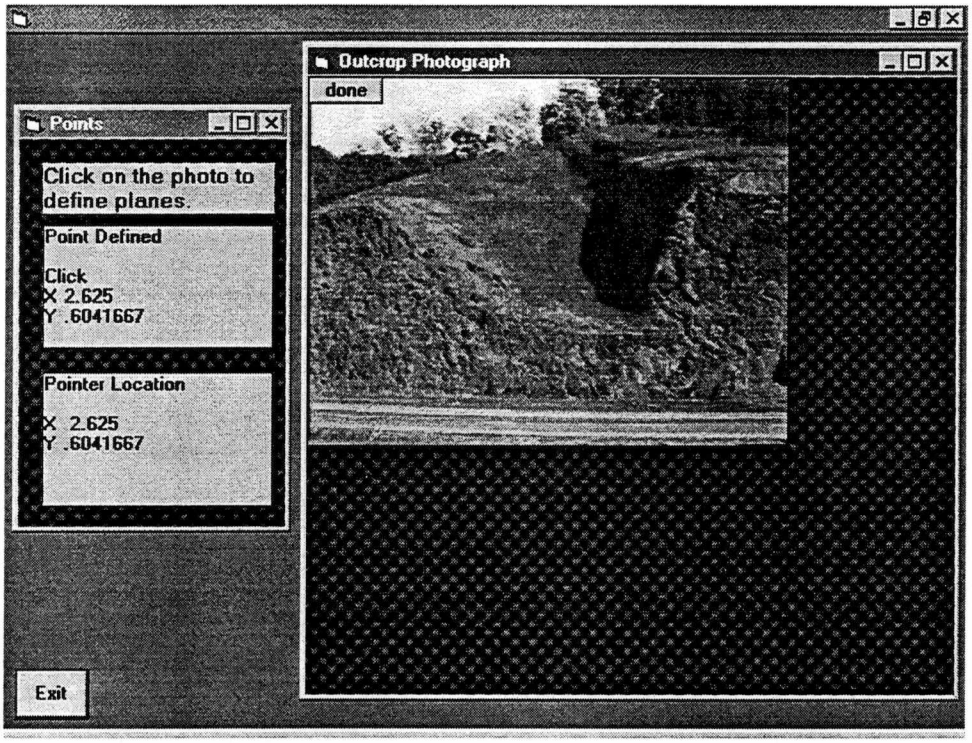


Figure 24 The selected image is displayed.

4. ***Defining Failure Surface on the Image***

The potential sliding surface trace on the outcrop is now defined by clicking at points along the bedding. The surface will be idealized as straight line segments between the points. The number of points, and hence the accuracy of the idealization, is determined by the user.

When clicking to define the surface, the points should always be chosen right to left. As the points are chosen, line segments will appear showing the surface, as shown in Figure 25. Pressing the *done* button in the upper left corner tells the program that the user is finished defining points.

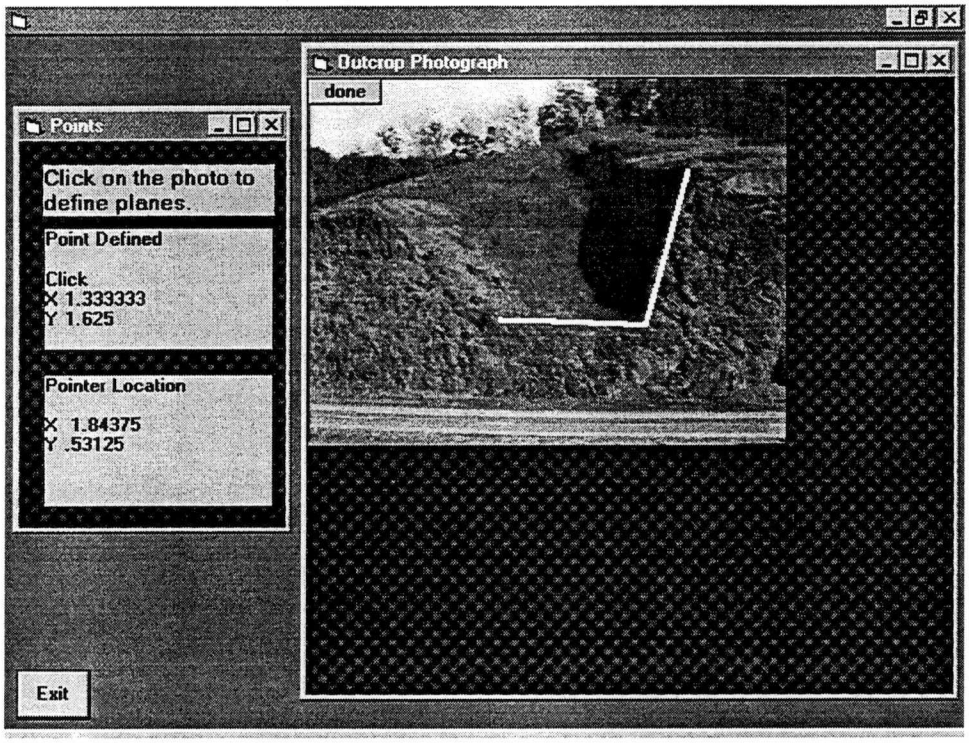


Figure 25 The failure surface is defined by clicking on points.

5. ***Reading Coordinates from a Text File***

As an alternative to loading a bitmap image, *ROCKSLIP* has the capability of reading coordinates directly from a text file, as mentioned earlier. This text file is created prior to running the program, saved as **.txt*, and loaded if that option is selected in the screen as shown in Figure 23. This text file can be created in *Windows Notepad* or *DOS Edit* and certain guidelines must be adhered to. The coordinate system is shown in Figure 26 and the coordinates must be entered from right to left, i.e. largest *X* first. The units are in inches, with the origin as shown. In the text file the first X value should be entered on the first line, the first Y value on the second line, the second X value on the third line, and so on. After this option is selected in the opening screen, another window opens to select

the file. After the file is selected, the coordinates will be displayed for confirmation by the user. An example file could be as follows,

```
1.7
0.55
1.4
1.1
0.6
1.1
0.4
0.45
```

which defines the three sided block in Figure 26, with the first coordinate at X_1 =1.7 and Y_1 =0.55, etc.

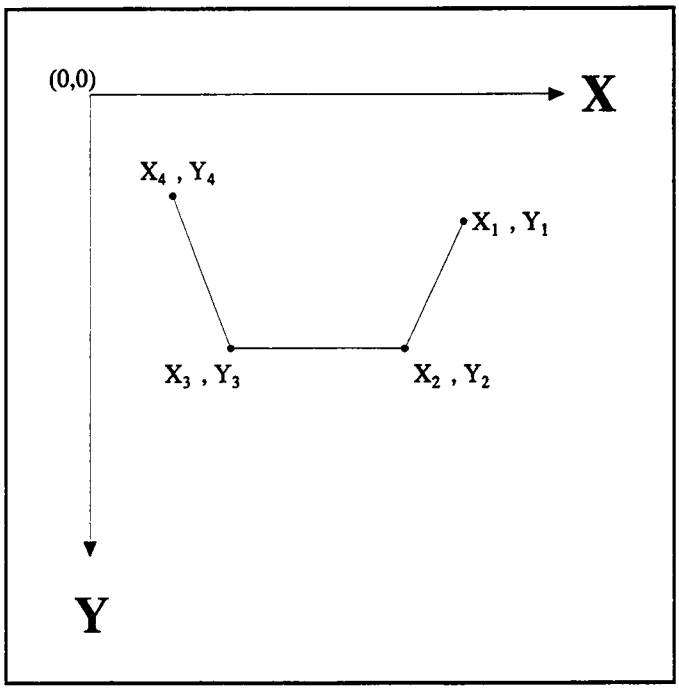


Figure 26 Coordinate system used in the input of points.

6. ***Defining the Fold Axis Orientation***

The remaining pieces of information that *ROCKSLIP* needs are the orientation of the fold axis of the structure that the user has defined and the orientation of the slope face. If the fold axis trend/plunge is already known, as from field estimation or graphical techniques, they may be entered directly by the selecting the *axis* button in the next window. The trend and plunge of the fold axis should be entered along with the dip and dip direction of the slope face, all in degrees azimuth.

The orientation of the axis of a fold may be determined graphically by two methods of stereographic projection described by Ramsay and Huber (1987) and Ramsay (1967). These methods are called the β-diagram and the π-diagram. The β-diagram technique relies upon the principle that each surface of a cylindrical fold contains the fold axis. If the measured surfaces of the fold are drawn on the projection their common intersection point will define a line common to all planes. This line is called the β-axis and should be parallel to the fold axis in space. If the fold is perfectly cylindrical and the measurements are made with no error, all great circles will intersect at one point and define one β-axis. In reality, neither of these conditions are met and multiple β-axes are produced, as in Figure 27. An average β-axis could then be determined to establish the fold axis. It is obvious that this technique is quite impractical for a large number of planes and therefore a π-diagram is more commonly used.

In the π-diagram method the normal vectors of all the plane measurements are plotted. If the fold is cylindrical then each of these poles is oriented at an angle of 90° from the fold axis. The poles will lie upon a great circle called the π-circle, as in Figure 28. The

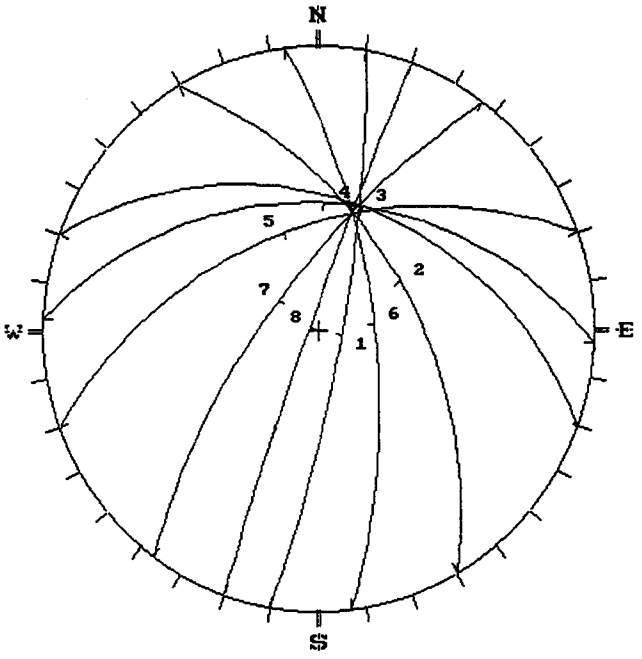


Figure 27 Lower hemisphere projection of eight planes of a fold and multiple β-axes.

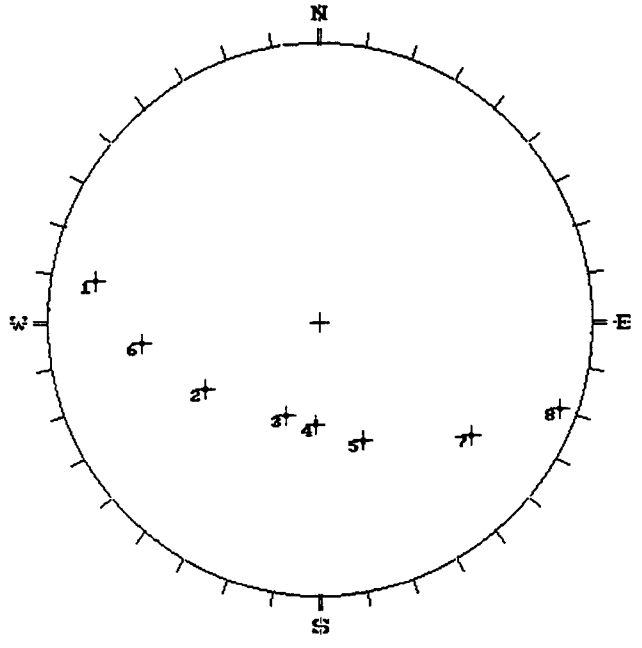


Figure 28 Lower hemisphere projection of the normal vectors of eight fold planes used to determine the π-axis.

perpendicular to this π-circle is plotted and called the π-axis. This π-axis lies parallel to the fold axis. Again, the fold will not be perfectly cylindrical and the measurements are not exact, producing some scatter. A best fit great circle is drawn and the orientation of its pole is taken as the fold axis orientation.

The user is also given the option of having *ROCKSLIP* calculate the fold axis orientation based upon dip/dip directions taken from the fold. These dip/dip directions are stored in a text file similar to the coordinates discussed earlier. Each line of this text file should contain a two digit dip followed by a space (or tab) and then three digit dip direction (azimuth). After this file is loaded the program uses a statistical technique proposed by Whitten (1966, pp. 582-585) to calculate the fold axis orientation. *ROCKSLIP* also tests the structure for cylindrical folding using criteria proposed by Ramsay and Huber (1987, pp. 333-336). These processes are discussed in Appendix A.

7. *Input Friction Angle*

After the fold axis orientation is input or calculated, *ROCKSLIP* asks for the angle of friction on the surface in question. This is entered in degrees, and an option will be presented later to change the angle.

8. *Correcting Cross Section*

In the same window with the friction angle, *ROCKSLIP* asks for the dip and dip direction of the slope face. The user is also asked if a true cross section was entered. The

true cross section is the section of the fold in the plane orthogonal to the fold axis. The model must be applied to the plane lengths and angles in the true cross-section. If yes is selected, there will be no correction for a true cross section. In this case the dip and dip direction of the free face need not be entered. If no is selected, the apparent cross section visible on the slope will be converted to the true section using the dip and dip direction of the slope face by a process described in Appendix A.

After the true cross-section is determined, the equations of the model are applied and the factor of safety is calculated for this structure. As shown in Figure 29, the factor of safety is given along with the true and apparent sections. After selecting the OK button the user is given the option of recalculating the factor of safety for different friction angles. Any number of angles may be analyzed, as in Figure 30.

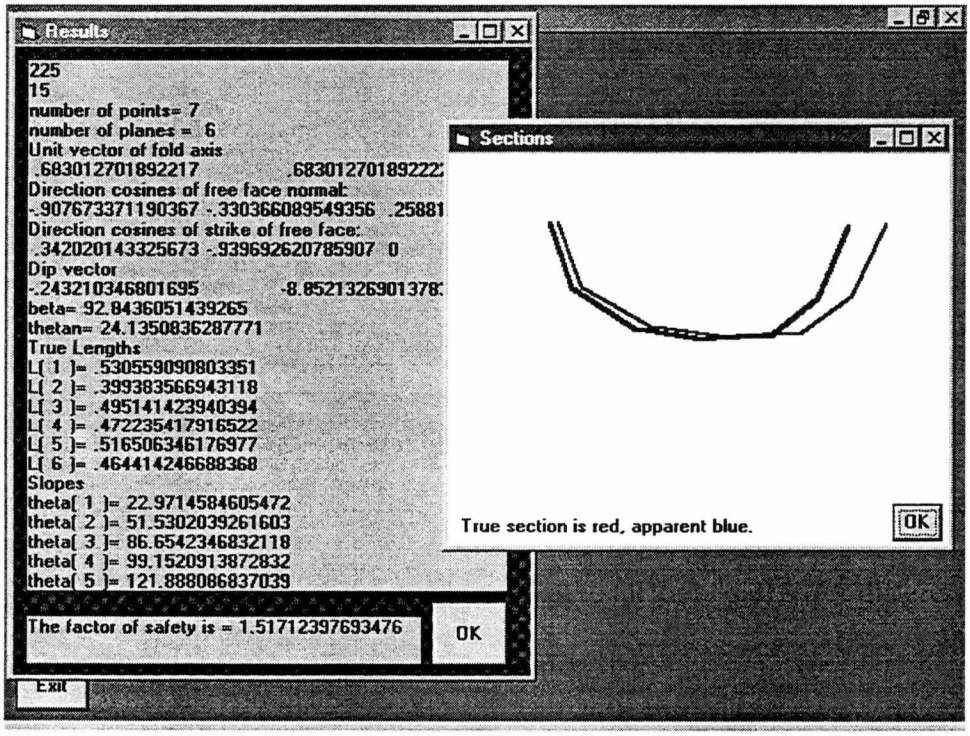


Figure 29 Final results are displayed including factor of safety and sections.

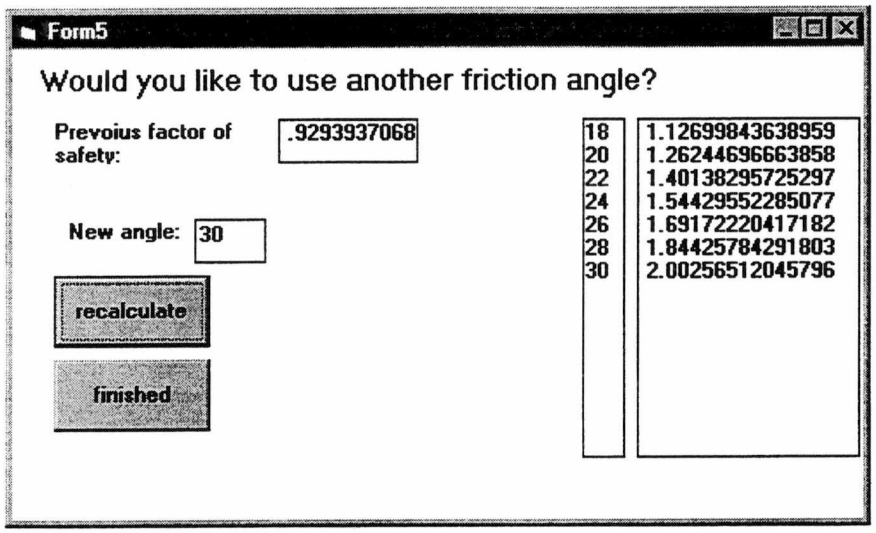


Figure 30 Recalculation of the factor of safety for different friction angles.

CHAPTER 7: CASE STUDY

Introduction

To demonstrate and test the model and computer program *ROCKSLIP* a study site was selected in East Tennessee for analysis. The site selected is a series of cut slopes along US Highway 19E near Biltmore in Carter County, upper East Tennessee (see Figure 31). The cuts were made through a thinly bedded Sevier Shale approximately ten years ago. Photographs of the study area can be seen in Appendix B.

Site Geology

The southern segment of the Appalachian Mountains can be divided into four belts or provinces (Rodgers, 1970). These are the Appalachian Plateau, Valley and Ridge, Blue Ridge, and the Piedmont Plateau, shown in Figure 32. The Appalachian Plateau province is characterized by flat-lying or nearly flat-lying sedimentary rocks, mainly Carboniferous. Some parts of the province are a true plateau, but more is dissected by deep, narrow valleys. The Blue Ridge province stretches from northern Georgia to southern Pennsylvania and forms the main divide of the Appalachians. This is the most mountainous area of the region, containing the Unaka and the Smoky Mountains, among others. The Piedmont Plateau is a nearly featureless upland plain underlain by crystalline schist, gneiss, and gneissic granite.

The Biltmore study site lies within the Valley and Ridge geologic province. This

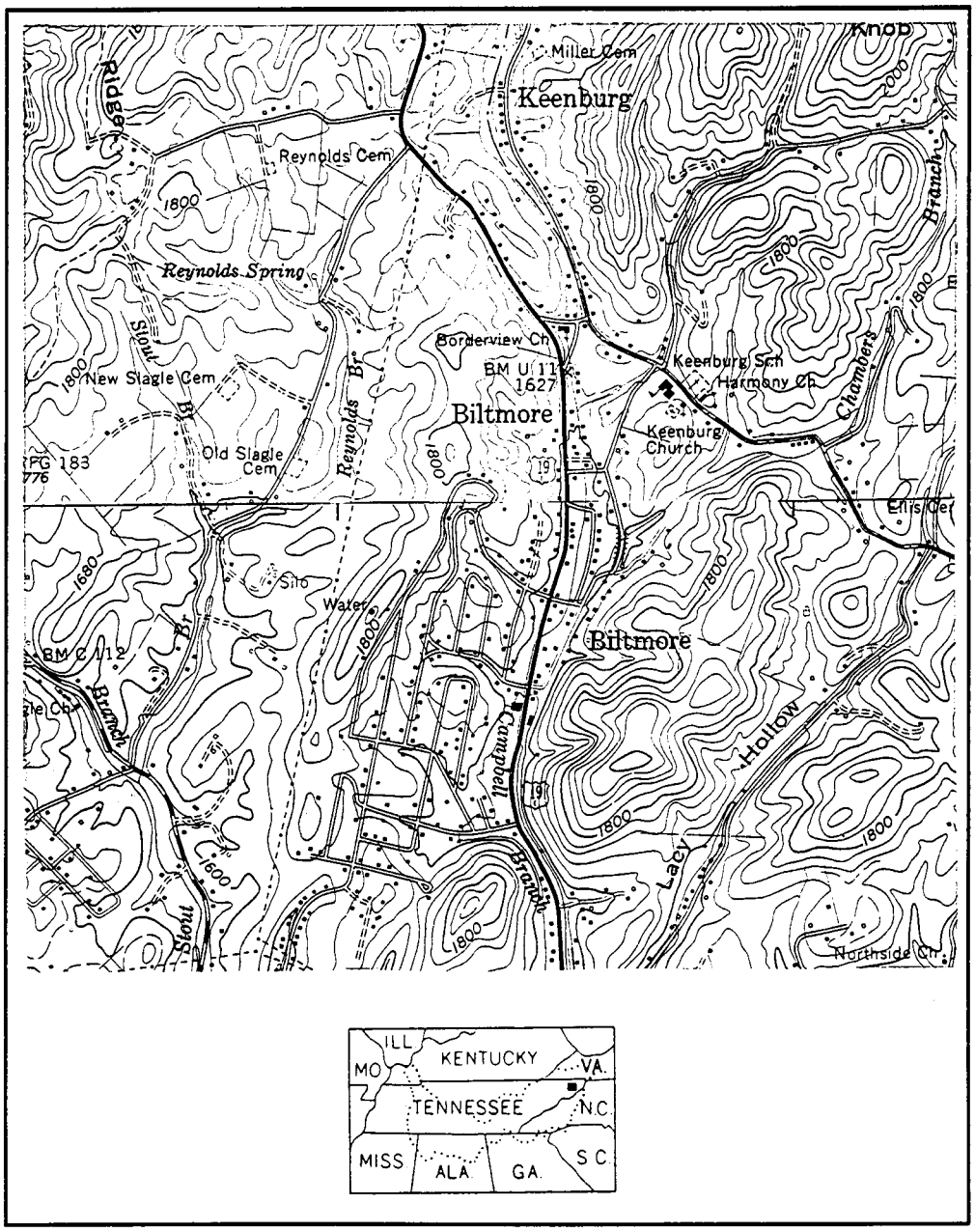


Figure 31 Study site location in Carter County, Tennessee (Elizabethton and Keenburg Quadrangles, 1969.)

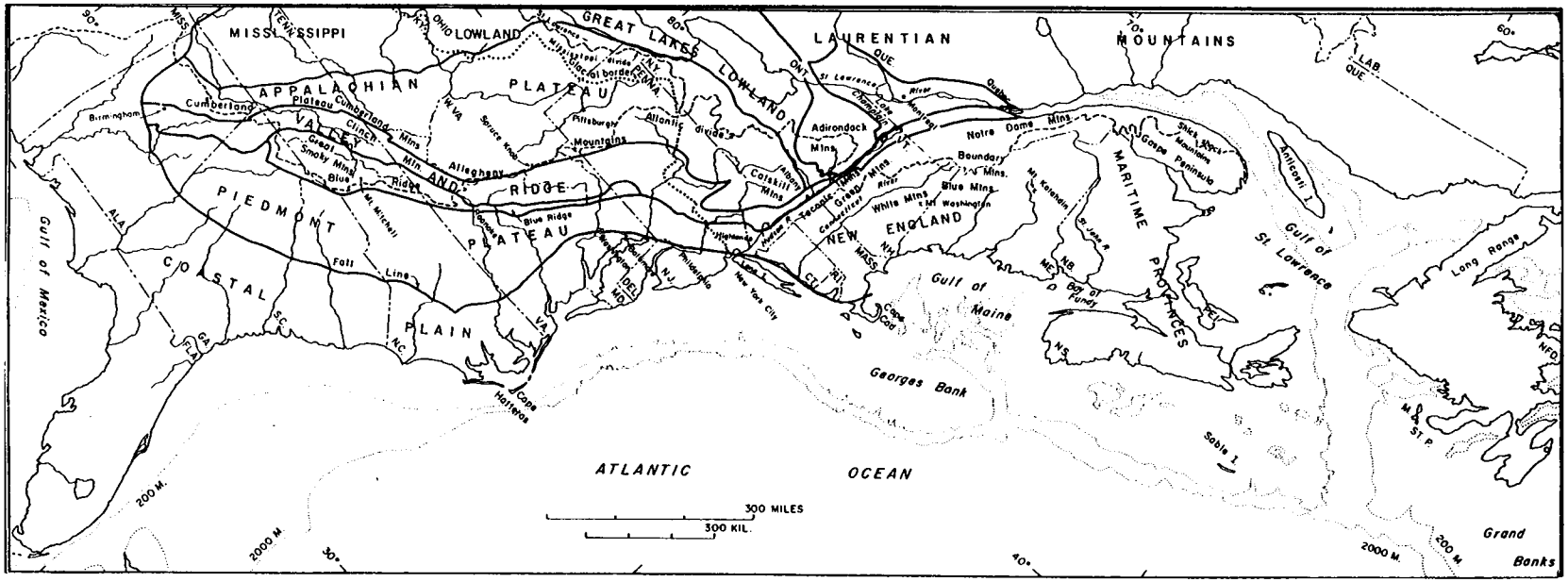


Figure 32 Geologic provinces of the Appalachians (Rodgers, 1970).

province is typified by narrow ridges, a kilometer or less across, persisting for tens or hundreds of miles. They are strictly parallel to each other and to the trend of the chain. Between the ridges are extensive parallel valleys, some narrow but others very broad. The province is underlain by a diversified sequence of Paleozoic sedimentary rocks (Cambrian to Carboniferous) that have been strongly folded and faulted with little metamorphism (Rodgers, 1970). These include limestone, sandstone, siltstone, shale, and dolomite. Nearly all rocks are faulted and tilted to the southeast, the direction of the massive tectonic forces that formed the structures. Figure 33 shows the many southeasterly dipping thrust faults of East Tennessee.

Several of these thrust faults are in Carter County, where the southeasterly dipping thrusts have produced folds at the study site with southwesterly trending fold axes. The Sevier Shale at the site is of Ordovician age (400 to 500 million years) and is of the Chickamauga Group. A generalized stratigraphic column is shown as Figure 34. It shows that the Sevier Shale has a thickness of 2000 to 7000 feet. This is a bluish-gray shale with thin gray limestone layers that can have yellowish weathered appearance. The rock at the site is thinly bedded, with layers no more than a few centimeters in thickness. Cleavage perpendicular to bedding is readily evident on the slopes. This additional plane of weakness results in small rock blocks spalling off the slopes, most of which are well less than a half meter across, but a few larger. Rock fences are used at the bases of some of the slopes to stop these blocks before they reach the roadway.

The particular slope chosen for analysis is an area of a past failure. This large syncline

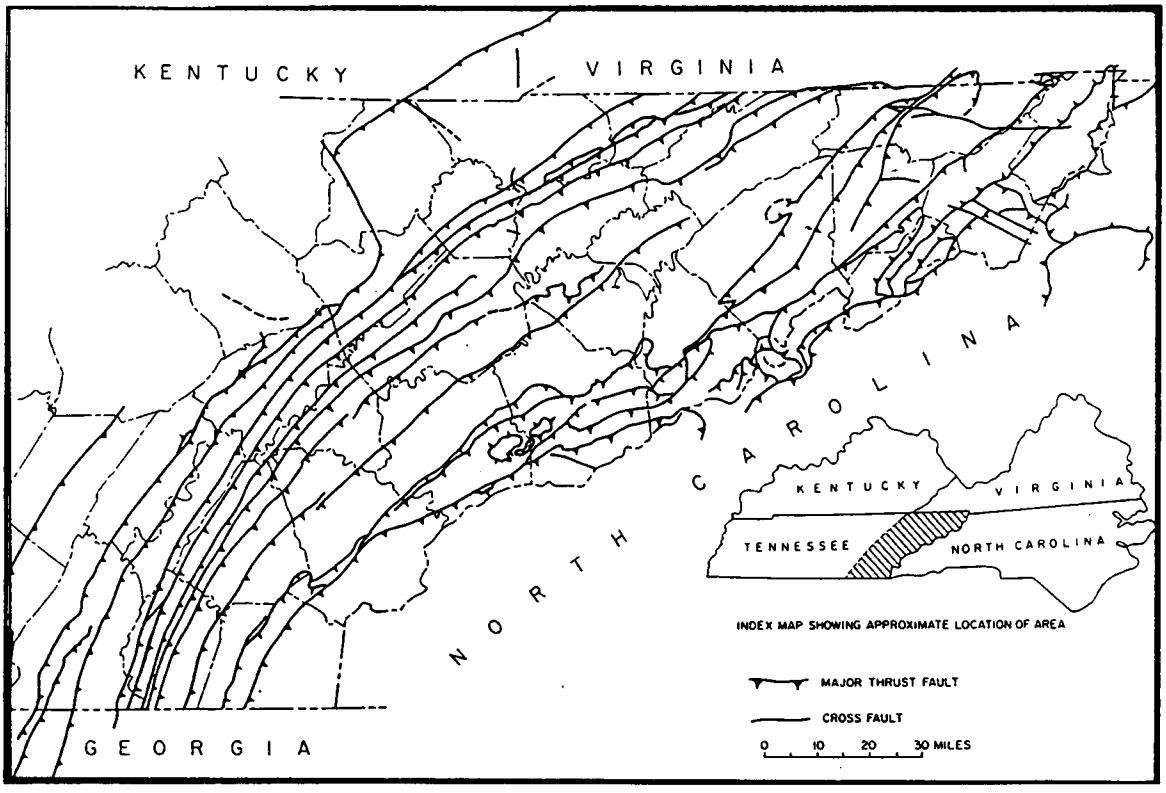


Figure 33 The major faults of East Tennessee, including Carter County (Thornbury, 1965).

GEOLOGIC PERIOD	FORMATION (THICKNESS IN FEET)
QUATERNARY	Recent Alluvium Loess (0-100)
TERTIARY	Claiborne Formation (200) Wilcox Formation (100) Porters Creek Clay (130-170), Clayton Formation (30-70) } Midway Group
CRETACEOUS	McNairy Sand (300) Coon Creek Formation (140) Coffee Sand (25-200)
PENNSYLVANIAN	Indian Bluff Formation (150-415) Slatestone Formation (500-750) Wartburg Sandstone (0-50), Glenmary Shale (50-150), Coalfield Sandstone (0-80), Burnt Mill Shale (110), Crossville Sandstone (30-50), Dorton Shale (150) } Crooked Fork Group Rockcastle Conglomerate (150-220), Vandever Formation (300-450), Newton Sandstone (90-200), Whitwell Shale (75-220), Sewanee Conglomerate (100-200) } Crab Orchard Mountains Group Signal Point Shale (0-180), Warren Point Sandstone (0-300), Raccoon Mountain Formation (0-200) } Gizzard Group
MISSISSIPPIAN	Pennington Formation (150-400) Bangor Limestone (70-400) Hartselle Formation (0-80) Monteagle Limestone - Ste. Genevieve Limestone (180-300) St. Louis Limestone (80-160) Warsaw Limestone (100-130) Fort Payne Formation (200)
DEVONIAN	Chattanooga Shale (24-50) Pegram Formation (0-30) Camden Formation (0-100) Harriman Formation (0-50) Flat Gap Limestone (0-13) Ross Formation (0-75)
SILURIAN	Rockwood Formation (350-600) } Clinch Sandstone (600) } Brownsport Formation (0-50), Wayne Group (0-140), Brassfield Limestone (0-50)
ORDOVICIAN	Shellmound (0-150), Arnheim Formation (0-20), Leipers Limestone (0-150), Inman Formation (0-50) } Sequatchie Formation (0-250) Cathevs Formation (50-125), Bigby Cannon Limestone (25-50), Hermitage Formation (50-150) } Nashville Group } Moccasin Formation } Bays Formation (1000) Carters Limestone (50-200), Lebanon Limestone (80-100), Ridley Limestone (90-150), Pierce Limestone (0-25), Murfreesboro Limestone (200-300), Pond Springs Formation (400) } Stones River Group } Chickamauga Supergroup } Sevier Shale (2000-7000) } Ottosee Shale (1000), Holston Formation (200-600), Lenoir Limestone (25-500) Mascot Dolomite (400-600), Kingsport Formation (250), Chepultepec Dolomite (1000), Copper Ridge Dolomite (1000) } Knox Group
CAMBRIAN	Maynardville Limestone (150-400), Nolichucky Shale (100-900), Maryville Limestone (300-800), Rogersville Shale (250), Rutledge Limestone (100-500), Pumpkin Valley Shale (100-600) } Conasauga Group } Honaker Dolomite (1500) Rome Formation (2000) Shady Dolomite (1000) Erwin Formation (1000-1500), Hampton Formation (500-2000), Unicoi Formation (2000-5000) } Chilhowee Group
PRECAMBRIAN	Sandsuck Formation (2000), Wilhite Formation (4000), Rich Butt Sandstone (1500) } Walden Creek Group } Ocoee Supergroup Pigeon Siltstone (10,000), Roaring Fork Sandstone (7000), Longarm Quartzite (5000), Wading Branch Formation (1500) } Snowbird Group } Ocoee Supergroup Basement Complex

Figure 34 Generalized Tennessee rock column (Wilson, 1981).

failed shortly after construction. The bedding is readily visible on the slope and it appears that the failure occurred generally along the curved bedding planes. The model and *ROCKSLIP* were applied here as "post-mortem" analysis, to determine if the failure could have been predicted and to determine the stability of the block that was there.

Orientation Data Analysis

The orientations of seventy bedding planes and bedding fractures were measured on the analyzed slope. The orientations were measured on December 1, 1995 by Scott Arwood and Doug Curl using a Brunton compass. This field work was performed in the morning and early afternoon in ideal weather conditions, clear and light winds. These data may be seen in Appendix B as Table 3. A lower hemisphere stereographic projection of the poles to these planes is shown in Figure 35. These poles lie approximately along a great circle, indicating that this may be a cylindrical fold. A weighted contour plot in Figure 36 further shows that the poles are grouped along a great circle. The orientation of the cut slope face was also measured for input into *ROCKSLIP*. The dip direction was found to be 225° azimuth and the dip to be 75° from horizontal.

An input file was created in order to calculate the orientation of the fold axis using *ROCKSLIP*. The program calculated a fold axis with a trend of 228° azimuth and a plunge of 11° from horizontal. Figure 37 shows the best fit great circle and the fold axis on a lower hemisphere projection as determined by *ROCKSLIP*. These values are very near the orientation determined by field estimation of 225° azimuth and 15°. The program also determined that this can be classified as a cylindrical fold.

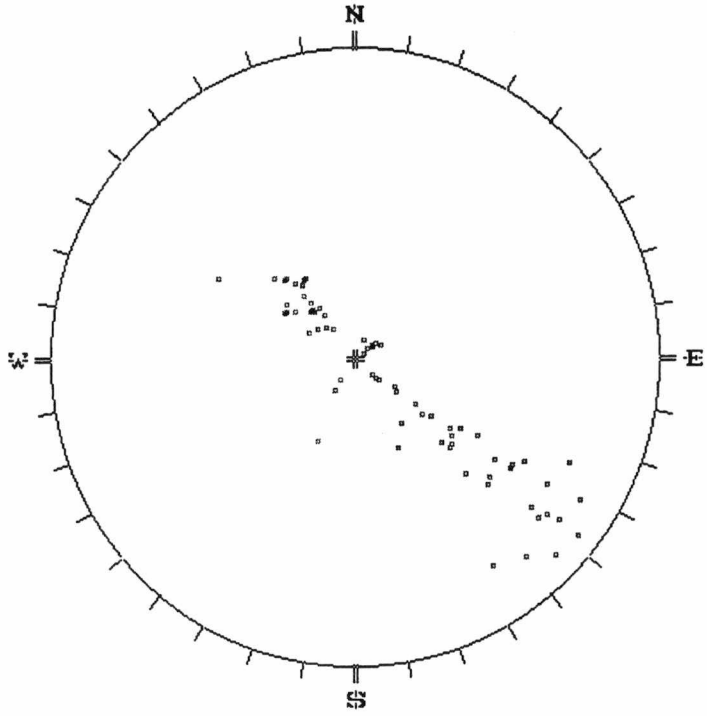


Figure 35 Lower hemisphere projection of the poles to the bedding.

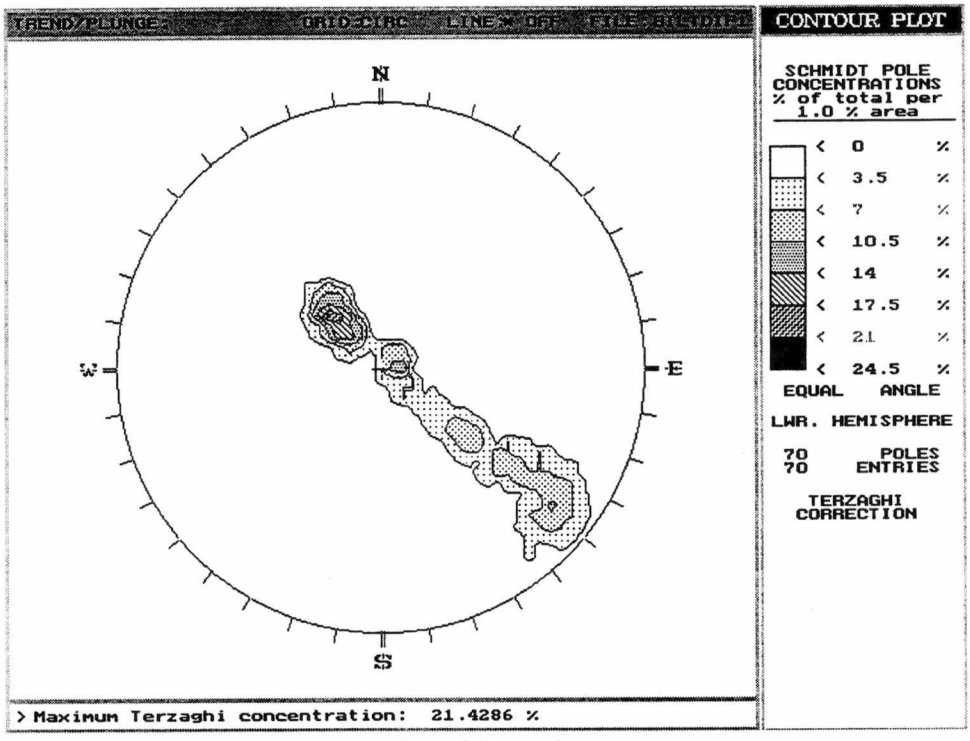


Figure 36 Weighted contour plot of the poles.

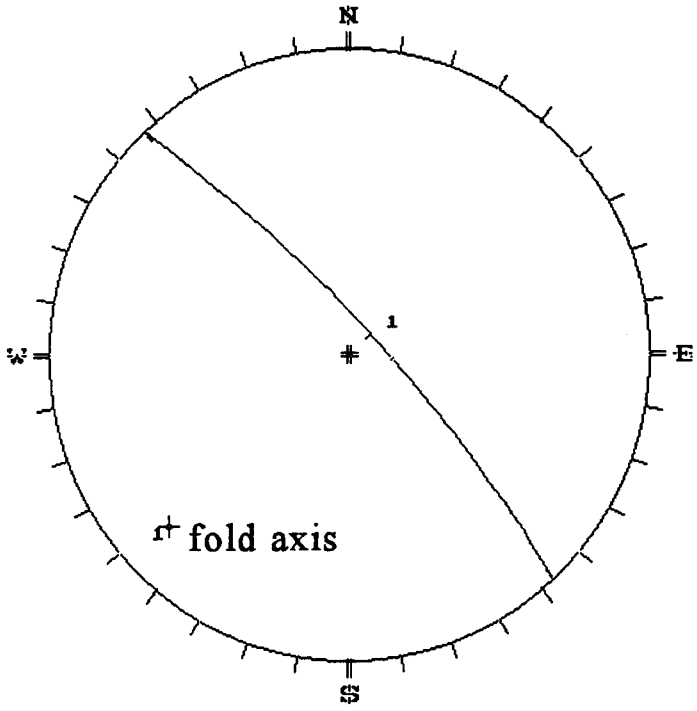


Figure 37 The best fit great circle and the fold axis.

Analysis

An image of the Biltmore slope similar to those of Appendix B was used in the *ROCKSLIP* analysis of the past failure surface of the slope. The curved surface of the failure block must be represented as a prismatic block with a finite number of planes in the program. The block was idealized as several different shapes for the sake of comparison, these were a two sided wedge, three sided block, and a five sided block. Different variations of each case were also used in the analysis. Figure 38 shows the three wedges, three 3-sided blocks, and three 5-sided blocks for which a factor of safety was calculated.

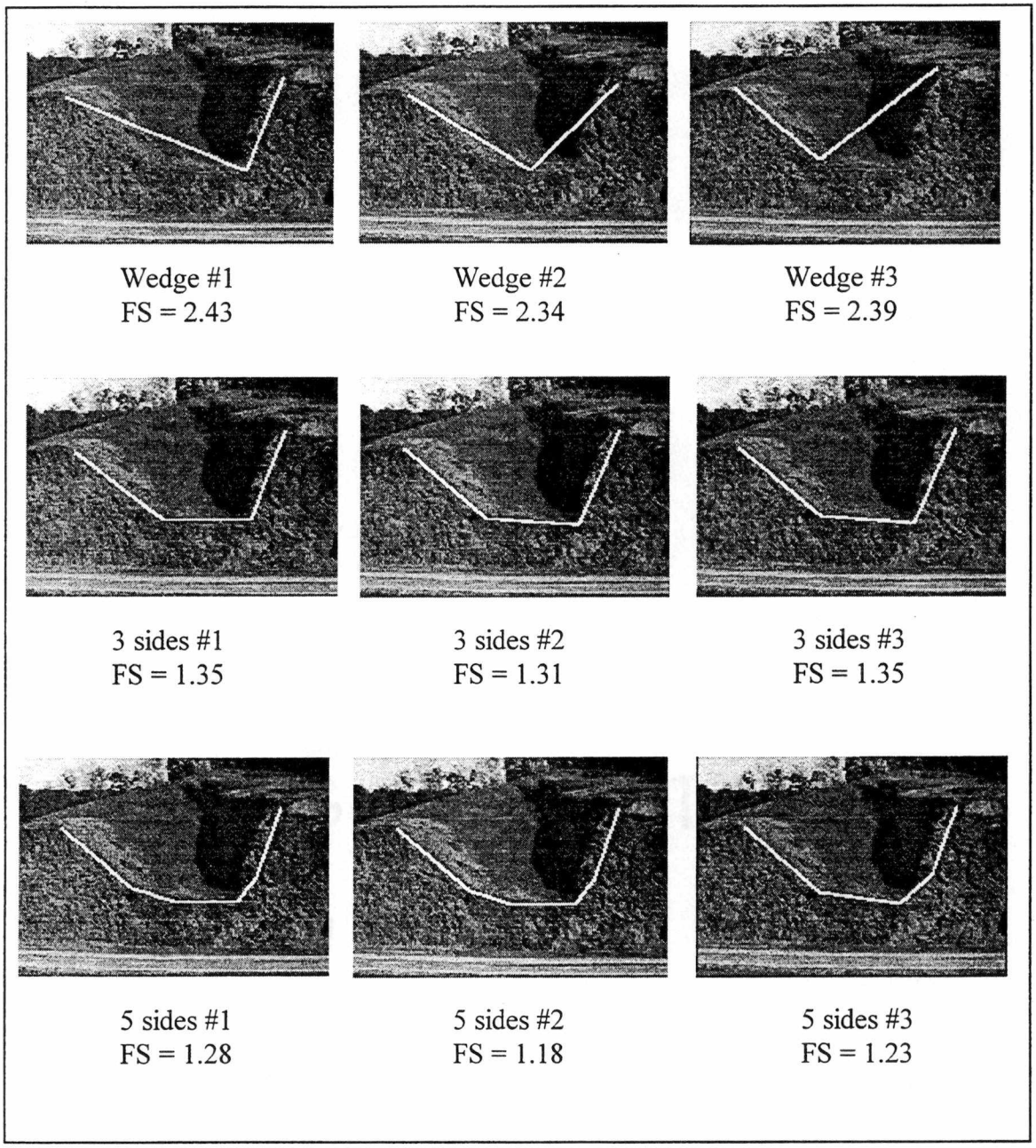


Figure 38 The failure surfaces, all with a fold axis plunge of 11° and a friction angle of 20°, used in the analysis of the Biltmore site with their factors of safety.

ROCKSLIP was run as described in Chapter 6 to analyze each of the nine failure blocks shown and also for a plane slide analysis. For each block the calculated fold axis and the measured slope face orientation were used as input. For the plane slide analysis, the dip of the plane was set equal to the plunge of the fold axis. The traces of the blocks were corrected to a true section using this information. The exact friction angle on the contact surfaces is unknown. Therefore, a range of friction angles was used, from 15° to 30°. Published angles for shale are in the range of 20° to 25°(Goodman, 1989; Hoek and Bray, 1981). Results of the analysis are shown graphically in Figure 39.

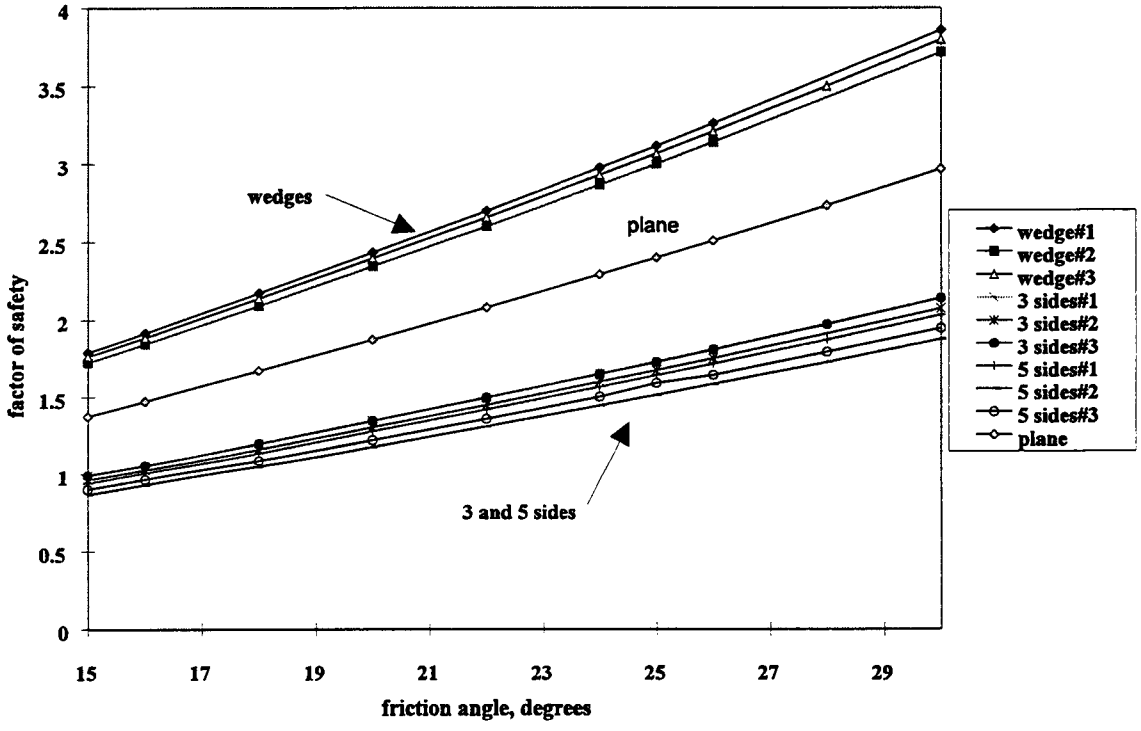


Figure 39 Factors of safety for each analysis of the Biltmore site for a range of friction angles.

Discussion

From Figure 39 it can be seen that the three wedge analyses are nearly the same, ranging from a low value between 1.5 and 2 to a high value over 3.5. The plane sliding analysis gave factors of safety less than the wedges, but above the three and five sided blocks. The wedge values are well above those of the three sided and five sided blocks, most in the range of 75 to 100 % higher. The factors of safety for these six blocks range from less than one at a friction angle of 15°, to a little less than two at a 30° friction angle. This demonstrates clearly that the wedge model overestimates the factor of safety and could lead to an unsafe design. The factors of safety for the five sided blocks are slightly lower than the three sided blocks, in the range of 5 to 10 % lower.

In Chapter 4 it was noted that the factor of safety for a block with a semicircular cross section is larger than a plane slide by a factor of $4/\pi$. For the Biltmore analysis it is shown that the plane slide analysis gives larger factors of safety than the three and five sided blocks. This may seem contradictory, but the difference is a result of the non-symmetry of the blocks of the Biltmore failure. To illustrate this effect, a block with three contact planes in Figure 40 will be used as an example. Plane 2 of this block is horizontal (parallel to the X axis), making $\theta_2=90°$. Resolving forces vertically and horizontally produces

$$N_1 \sin\theta_1 + N_2 + N_3 \sin\theta_3 = R_N \qquad (77)$$

and

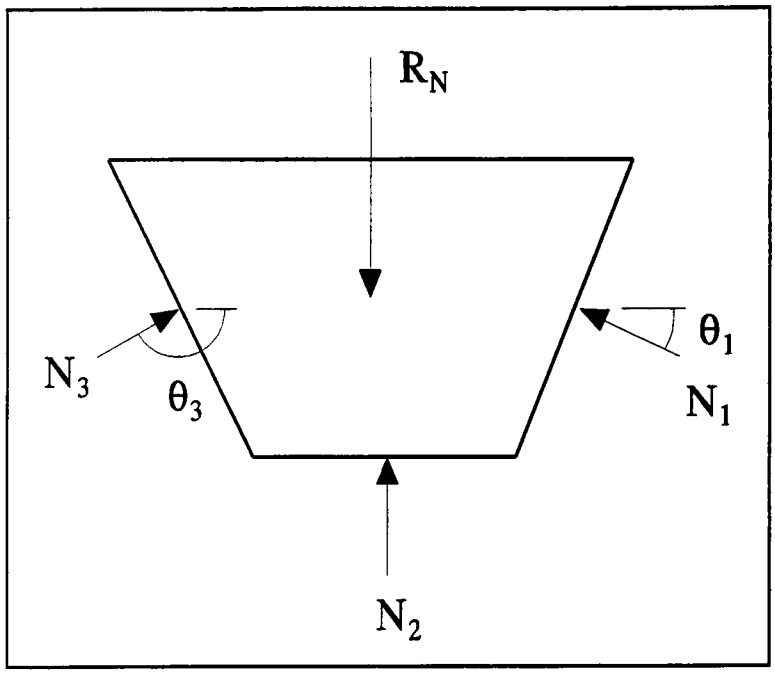


Figure 40 Three sided block with plane 2 horizontal used in the discussion.

$$N_1 \cos\theta_1 = N_3(-\cos\theta_3) \quad . \tag{78}$$

Solving (78) for N_3, substituting into (77), and simplifying produces

$$N_1\left(\frac{\sin\theta_1\cos\theta_3 - \sin\theta_3\cos\theta_1}{\cos\theta_3}\right) + N_2 = R_N \quad . \tag{79}$$

The total amount of frictional resistance is a function of the sum of the normal forces.

This sum may be expressed from (79) as

$$\sum N_i = N_1 + N_2 + N_3 = R_N + N_3 + (1-\alpha)N_1 \tag{80}$$

where α represents the quantity within the parentheses of (79). The quantity $(1-\alpha)$ may

be expressed as

$$\beta = \frac{\cos\theta_3 - \sin\theta_1 \cos\theta_3 + \cos\theta_1 \sin\theta_3}{\cos\theta_3} . \qquad \textbf{(81)}$$

From Equation (80) it can be seen that the quantity β is directly proportional to the sum of the normal forces, and therefore the resisting forces also. A graph of the function β is shown as Figure 41. The three dimensional plot forms a saddle with the line of the symmetric sections forming the ridge (i.e., for a symmetric section $\theta_3=\pi-\theta_1$). The maximum value of β occurs at $\theta_1=0$ and $\theta_3=\pi$ (a rectangular section). It can be seen that β decreases when plane 1 is steeper than plane 3, or vice versa. The plane slide analysis is, therefore, a lower bound only when dealing with symmetric sections, not with non-symmetric sections.

The factors of safety for the three and five surfaced prismatic blocks are less than the desirable 1.5 up to a friction angle of about 25°. This indicates that this slope, and in particular this block, is potentially unstable. Therefore, it can be concluded that this past failure could have been predicted using this model. It should also be noted that this analysis did not include a consideration of water forces, which would only reduce the factor of safety further.

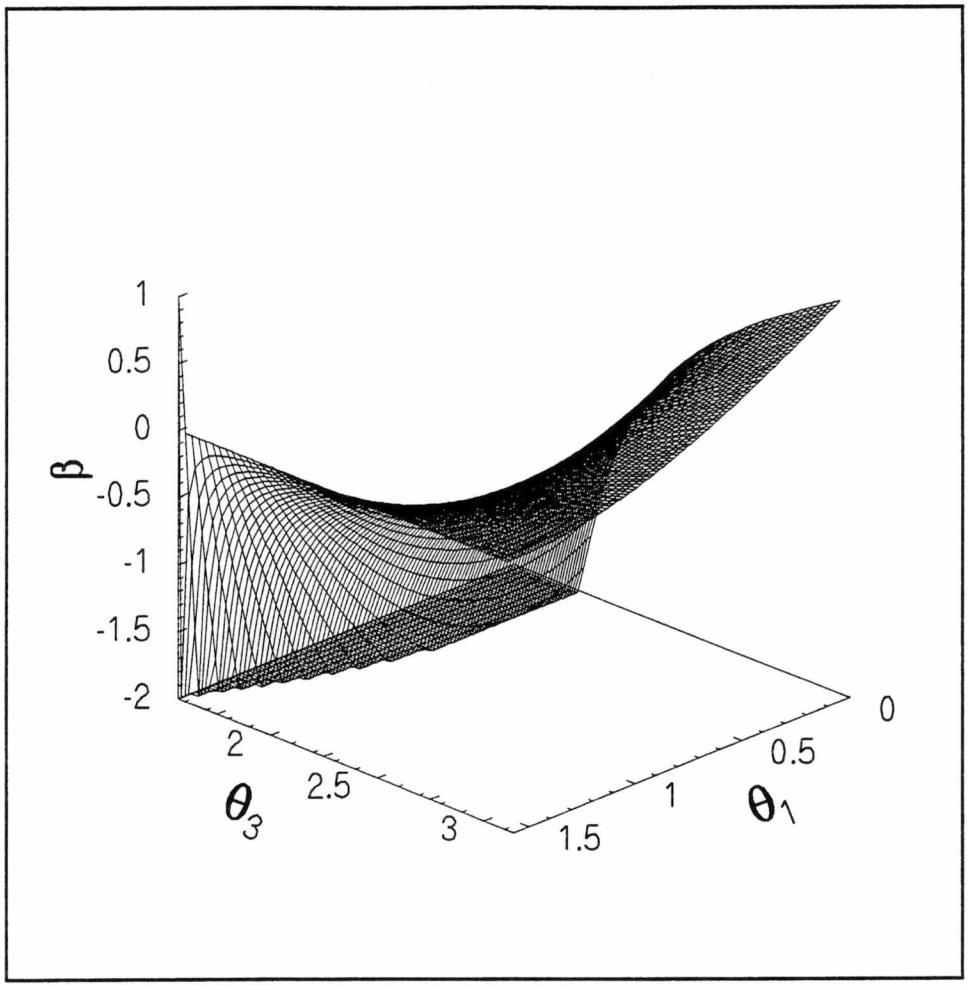


Figure 41 Graph of β as a function of the angles of planes 1 and 3.

CHAPTER 8: CONCLUSIONS

The analysis of slope stability in folded sedimentary rocks presents unique problems and situations which to date have not been adequately dealt with in the geotechnical literature. The folding of the bedding planes produces potential failure blocks with curved sliding surfaces. Traditional limiting equilibrium stability techniques are capable of the analysis of plane and wedge failures only. These one and two sided blocks are not adequate to model a slope failure in folded rocks. The main purpose of this ongoing research program is to develop a model for the sliding stability of folded rock blocks and to develop a computer program to implement this model.

The first step was the development of an energy model to analyze the stability of a prismatic rock block with *m* sides. The modeled elastic conservative system was used to find the distribution of normal forces which minimized the potential energy. Once found, these normal forces are used to calculate the frictional resistance to sliding. The model was then extended to cylindrical blocks with curved sliding surfaces. This model was presented in a general form, and for special cases of circular and elliptical cylinders. Cohesion on the contact planes was also added at this point. The model was then validated and analyzed against the limiting equilibrium methods for special cases.

A major part of this research program was the development of a computer program to implement the model. The nature of the prismatic block equations makes a hand calculation of a factor of safety quite laborious. The *Windows* program *ROCKSLIP* uses an image of the slope as its major source of input along with field data from the rock

mass. The operation of the program was described along with the mathematical processes involved in the calculation of a factor of safety.

Finally, a case study from East Tennessee was presented. A slope with a cylindrical fold in shale was analyzed. The slope was an area of a previous failure, with the failure occurring along bedding planes in a syncline. The model and computer program were applied to this slope as a demonstration and test. Results indicated that this failure could have possibly been predicted.

In summary, a new model and computer program for slope stability in folded rocks have been presented. This model can calculate the factor of safety against sliding for a prismatic or cylindrical rock block, commonly produced in folded rocks. The model has been tested and demonstrated with favorable results and has been shown to have great utility.

REFERENCES

REFERENCES

Barton, N.R., Bandis, S., and Bakhtar, K. (1985). "Strength, Deformation and Conductivity Coupling of Rock Joints." *Int. J. Rock Mech. Min. & Geomech. Abstr.* 22, 121-140.

Brady, B.H.G. and Brown, E.T. (1993). *Rock Mechanics for Underground Mining.* Chapman & Hall, London, 2nd ed.

Chan, H.C. and Einstein, H.H. (1981). "Approach to Complete Limit Equilibrium Analysis for Rock Wedges - The Method of Artificial Supports." *Rock Mechanics.* 14, 59-86.

Desai, C.S. (1979). *Elementary Finite Element Method.* Prentice-Hall, Englewood Cliffs, New Jersey.

Franklin, J.A. and Dusseault, M.B. (1989). *Rock Engineering.* McGraw-Hill, New York.

Goodman, R.E. (1989). *Introduction to Rock Mechanics.* Wiley, New York, 2nd ed.

Goodman, R.E. (1976). *Methods of Geological Engineering in Discontinuous Rocks.* West Publishing, St. Paul.

Herget, G. (1988). *Stresses in Rock.* A.A. Balkema, Rotterdam.

Hoek, E. and Bray, J. (1981). *Rock Slope Engineering.* Institute of Mining and Metallurgy, London.

John, K.W. (1968). "Graphical Stability Analysis of Slopes in Folded Rocks." *Proceedings American Society of Civil Engineers.* 94(SM2), 47-52.

Londe, P., Vigier, G. and Vormeringer, R. (1969). "Stability of Rock Slopes, a Three-Dimensional Study." *Proceedings American Society of Civil Engineers.* 9(SM1), 235-262.

Londe, P., Vigier, G. and Vormeringer, R. (1970). "Stability of Rock Slopes - Graphical Methods." *Proceedings American Society of Civil Engineers.* 96(SM4), 1411-1434.

Mauldon, M. and Ureta, J. (1996). "Stability Analysis of Rock Wedges with Multiple Sliding Surfaces." *Geotechnical and Geological Engineering.* 14, 51-66.

Mauldon, M. and Ureta, J. (1995). "Sliding Stability of Prismatic Blocks." *Rock Mechanics Proceedings of the 35th US Symposium.* A.A. Balkema, Rotterdam, 39-44.

Ramsay, J.G. (1967). *Folding and Fracturing of Rocks.* McGraw-Hill, New York.

Ramsay, J.G. and Huber, M.I. (1987). *The Techniques of Modern Structural Geology, Volume 2: Folds and Fractures*. Academic Press Limited, San Diego.

Rodgers, John (1970). *The Tectonics of the Appalachians.* John Wiley & Sons, New York.

Seattle Filmworks. 1260 16th Avenue West, Seattle WA 98119, 1-800-FILMWORKS.

Spiegel, M.R. (1968). *Mathematical Handbook of Formulas and Tables.* McGraw-Hill, New York.

Thornbury, W.D. (1965). *Regional Geomorphology of the United States.* John Wiley & Sons, New York.

Turner, A.K. and Schuster, R.L. (1996). *Landslides, Investigation and Mitigation.* Transportation Research Board Special Report 247. National Academy Press, Washington, D.C.

Ureta, J.A. (1994). "Stability Analysis of Prismatic Rock Blocks." Master's Thesis, Dept. of Civil & Environmental Engineering, University of Tennessee, Knoxville.

Whitten, E.H.T. (1966). *Structural Geology of Folded Rocks*. Rand McNally & Co., Chicago.

Wilson, R.L. (1981). *Guide to the Geology Along the Interstate Highways in Tennessee.* Tennessee Division of Geology Report of Investigations 39.

APPENDICES

APPENDIX A

Mathematical Algorithm of *ROCKSLIP*

Input Variables

The following quantities are input by the user and saved as variables:

Quantity	Saved as
points on failure surface	XC(i), YC(i) ... XC(n), YC(n)
trend of fold axis	TR
plunge of fold axis	PL
outcrop dip	OD
outcrop dip direction	ODD
friction angle	phi

Calculation Algorithms

1. Calculate Vectors

A. Find the direction cosines, lf, mf and nf, of outcrop unit normal based upon a global coordinate system of X east, Y north and Z up:

lf = sin(OD) sin(ODD)

mf = sin(OD) cos(ODD)

nf = cos(OD)

B. Find the direction cosines, P, Q and R, of fold axis vector:

P = cos(PL) sin(TR)

Q = cos(PL) cos(TR)

R = sin(PL)

Check to see if fold axis vector is downward (i.e., R<0), if not, take the opposite direction, by changing the sign of P, Q, and R.

C. Find the direction cosines, ls, ms and ns, of the strike of the free face:

ls = -cos(ODD)

ms = sin(ODD)

ns = 0

2. Transform apparent section to true section

The apparent cross section of the failure surface that appears on the slope face must be transformed to a true cross section before the model may be applied and the factor of safety calculated. As shown in Figure 42, the section that appears on the slope is not, in general, the true section because the face is not orthogonal to the line of intersection **I**. Also shown is the normal to the slope face, $\mathbf{n}_f$. The line AA' in Figure 42 is found from the orthogonal projection of **I** on the slope face, and BB' is then perpendicular to AA'. To obtain the true section, the lengths parallel to BB′ are unchanged. The lengths parallel to AA′ are, however, shortened by a factor of cos θ, where θ is the angle between the slope face normal and the line of intersection, as shown in Figure 42. The true length in the AA′ direction is $L=L'\cos\theta$.

To convert the coordinates recorded by the program from the apparent section to the corresponding true section coordinates, an axis transformation routine is employed. The points recorded in an XY coordinate system on the apparent section are converted to an

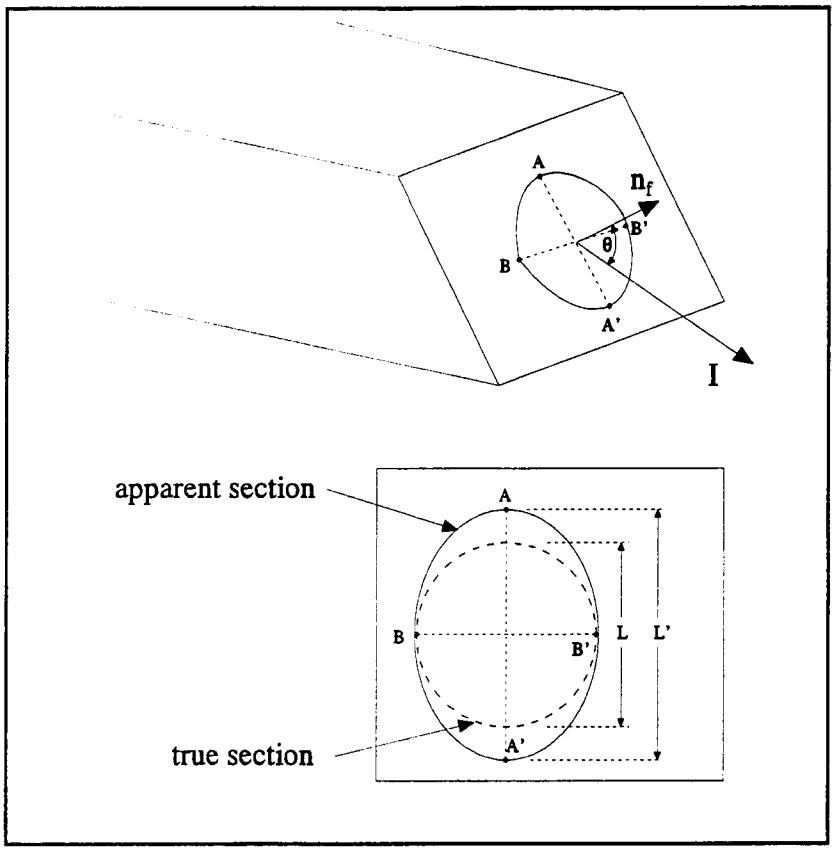


Figure 42 Apparent and true sections on a slope face.

X′Y′ system, where Y′ is parallel to the orthogonal projection of the intersection vector on the slope face (i.e., parallel to AA′). The coordinate systems are shown in Figure 43.

The position of y' can be found in the XY system as

$$y' = \frac{y}{\cos\beta} + (x - y\tan\beta)\sin\beta = \frac{y}{\cos\beta} + x\sin\beta - y\frac{\sin^2\beta}{\cos\beta} = x\sin\beta + y\cos\beta \qquad \textbf{(82)}$$

and x' is

$$x' = x\cos\beta - y\sin\beta \ . \qquad \textbf{(83)}$$

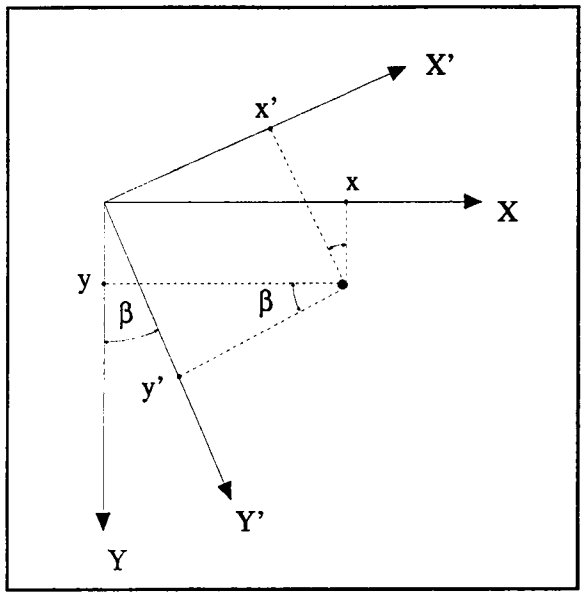


Figure 43 Coordinate axes used in the transformation of the apparent section.

These two expressions give the coordinates of a point (x, y) in the X′Y′ system. The next step is to find the coordinates (x'', y'') of the corresponding point in the true cross section. This can be found by shortening the y' coordinates by a factor of cosθ, and leaving the x' coordinates unchanged, yielding

$$\begin{aligned} x'' &= x' \\ y'' &= y' \cos\theta \ . \end{aligned} \tag{84}$$

Finally we must convert points on the true section back into the original coordinate system. The appropriate transformation can be found by solving (82) and (83) for x and y. The coordinates (x''', y''') in the true section with respect to the XY system are

$$\begin{aligned} x''' &= x'' \cos\beta + y'' \sin\beta \\ y''' &= -x'' \sin\beta + y'' \cos\beta \ . \end{aligned} \tag{85}$$

To implement this in *ROCKSLIP*, increments between the points are utilized. That is, in

equations (82-85) the x is replaced by deltax(i) and y replaced by deltay(i), where deltax(i) = XC(i) - XC(i-1) and deltay(i) = YC(i) - YC(i-1). The other coordinates, x', y', etc. are replaced similarly by deltaxp(i), deltayp(i), etc.

After calculating deltax and deltay for each point, the next step is to calculate the angle β. The process is:

A. Find the direction cosines ld, md and nd, of the dip vector:

ld = cos(OD) sin(ODD)

md = cos(OD) cos(ODD)

nd = sin(OD)

B. Find the direction cosines of the vector AA′ from the dot product between the fold axis vector and the unit normal vector.

C. Calculate β as the arc cosine of the dot product between the dip vector and vector AA′.

Next, the angle θ is calculated as the arc cosine of the dot product between the fold axis vector and the unit normal vector. Next, deltaxp(i) through deltaxppp(i) are calculated for each point. The true coordinates for each point are then

XT(i) = deltaxppp(i) + XT(i-1)

YT(i) = deltayppp(i) + YT(i-1).

The true plane lengths are then calculated as LT(i). The angle θ_i of each plane is calculated by first finding the slope of the line based upon the true coordinates, and then calculating the angle from the slope.

3. Find the Remaining Variables

If the user chose the option of having the program calculate a fold axis orientation, it is now calculated. This calculation is based upon the π-diagram technique discussed earlier in Chapter 6. When performed by hand on a stereographic projection a best fit great circle is drawn through the poles of the measured planes. *ROCKSLIP* uses a statistical technique described by Whitten (1966) to determine this best fit great circle. The procedure is as follows:

The normal to the ith measured plane has direction cosines l_i, m_i, and n_i. When plotted on a stereographic projection the normals lie on a great circle, if the fold is cylindrical. The normal to this great circle plane is the fold axis, which has direction cosines x, y and z, the unknowns at this point. Taking the dot product between the ith normal and the fold axis produces

$$l_i x + m_i y + n_i z = k \qquad \textbf{(86)}$$

where $k = \cos\theta$, θ being the angle between the fold axis and the ith normal plane. For a perfectly cylindrical fold, each normal of the measured planes will be oriented at $\theta = \pi/2$ from the fold axis and k will equal zero. In reality, there will be a different k for each normal, generally none with k =0. The direction cosines are calculated from the input field data as

l_i = sin(dip) sin(dipdirection)

m_i = sin(dip) cos(dipdirection)

n_i = cos(dip) .

With the numerous orientations that are measured, Equation (86) is solved by the standard method of least squares. Rewriting Equation (86) produces the equation

$$l_i = \frac{k}{x} - \frac{y}{x} m_i - \frac{z}{x} n_i \tag{87}$$

in which l_i can be considered a measured value and the right side of the equation a calculated value. Then, the sum of the squares of the differences between the measured l_i and its calculated value is

$$\sum_{i=1}^{N} \left(l_{i_{measured}} - l_{i_{calculated}} \right)^2 = \sum_{i=1}^{N} \left(l_i - \frac{k}{x} + \frac{y}{x} m_i + \frac{z}{x} n_i \right)^2 \tag{88}$$

where N is the number of planes measured. To obtain the least squares solution the sum of squares is minimized. If Equation (88) is expressed as the function F, to minimize this function it is necessary that

$$\frac{\partial F}{\partial \frac{k}{x}} = \frac{\partial F}{\partial \frac{y}{x}} = \frac{\partial F}{\partial \frac{z}{x}} = 0 \tag{89}$$

These partial derivatives produce three equations,

$$\frac{\partial F}{\partial \frac{k}{x}} = \sum_{i=1}^{N} 2\left(l_i - \frac{k}{x} + \frac{y}{x}m_i + \frac{z}{x}n_i\right)\cdot(-1) = 0$$
$$\frac{\partial F}{\partial \frac{y}{x}} = \sum_{i=1}^{N} 2\left(l_i - \frac{k}{x} + \frac{y}{x}m_i + \frac{z}{x}n_i\right)\cdot(m_i) = 0 \qquad \textbf{(90)}$$
$$\frac{\partial F}{\partial \frac{z}{x}} = \sum_{i=1}^{N} 2\left(l_i - \frac{k}{x} + \frac{y}{x}m_i + \frac{z}{x}n_i\right)\cdot(n_i) = 0$$

These three equations and four unknowns can be written in matrix form as

$$\begin{bmatrix} N & \sum m_i & \sum n_i \\ \sum m_i & \sum m_i^2 & \sum m_i n_i \\ \sum n_i & \sum m_i n_i & \sum n_i^2 \end{bmatrix} \begin{bmatrix} \frac{k}{x} \\ -\frac{y}{x} \\ -\frac{z}{x} \end{bmatrix} = \begin{bmatrix} \sum l_i \\ \sum l_i m_i \\ \sum l_i n_i \end{bmatrix} . \qquad \textbf{(91)}$$

Each of the terms involving the direction cosines is calculated by the program. Then the 3 x 3 matrix, called **Q**, is inverted to solve for the unknowns,

$$\begin{bmatrix} \frac{k}{x} \\ -\frac{y}{x} \\ -\frac{z}{x} \end{bmatrix} = Q^{-1} \begin{bmatrix} \sum l_i \\ \sum l_i m_i \\ \sum l_i n_i \end{bmatrix} \qquad \textbf{(92)}$$

An additional equation is provided by the Pythagoras theorem

$$x^2 + y^2 + z^2 = 1 \qquad \textbf{(93)}$$

which allows the calculation of the four unknowns. The orientation of the fold axis is then calculated as

$$\text{plunge} = \sin^{-1}(z)$$

$$\text{trend} = \sin^{-1}\left(x / \cos(\text{plunge}) \right)$$

and then these values can be used in the factor of safety calculation. *ROCKSLIP* also tests the fold to determine if it is cylindrical or not. Ramsay and Huber (1987) suggest that if more than 90% of the poles fall within an angle of 10° from the best fit great circle, then the fold should be termed cylindrical.

The remaining variables not yet found are the angles δ and θ_u^*. The angle δ is the arc cosine of the dot product between the fold axis vector and the weight vector. Equation (76) is solved to find θ_u^* using the true plane lengths and angles previously determined. Equation (76) cannot be solved directly, therefore a root solving routine (one point iteration) is used to solve the function

$$F(\theta_u^*) = \frac{\sum_{i \in A} L_i \cos(\theta_u^* - \theta_i) \sin(\theta_u^* - \theta_i)}{\sum_{i \in A} L_i \cos^2(\theta_u^* - \theta_i)} - \tan(\theta_u^* - \theta_r) = 0 \qquad (94)$$

for θ_u^*.

4. Calculate the Factor of Safety

The factor of safety is then calculated using Equation (75) based upon the properties of the true section (i.e., the true lengths LT(i) and the true angles θ_i), the input friction angle, and the calculated θ_u*. The factor of safety is given on the screen, as well as an outline of the apparent and true sections, drawn from the apparent and true coordinates.

APPENDIX B

Photographs and Field Data of the Biltmore Study Site

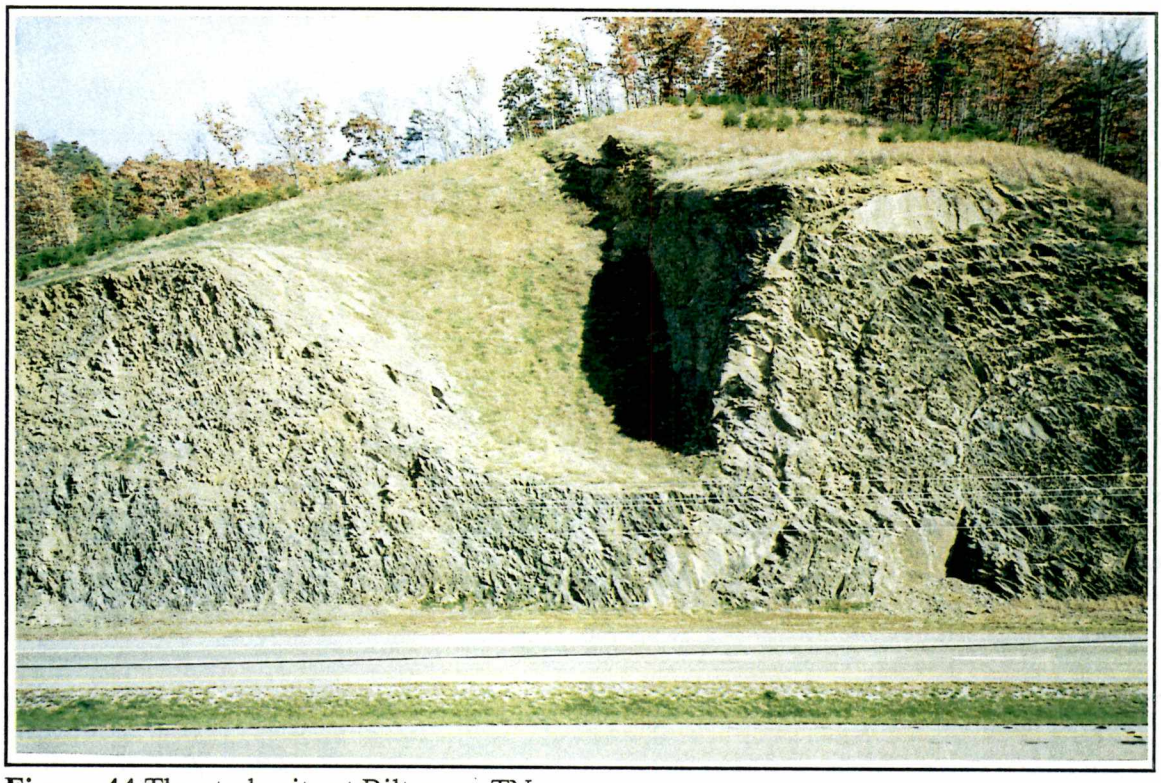


Figure 44 The study site at Biltmore, TN.



Figure 45 The bedding planes can be seen to the right of the failure.

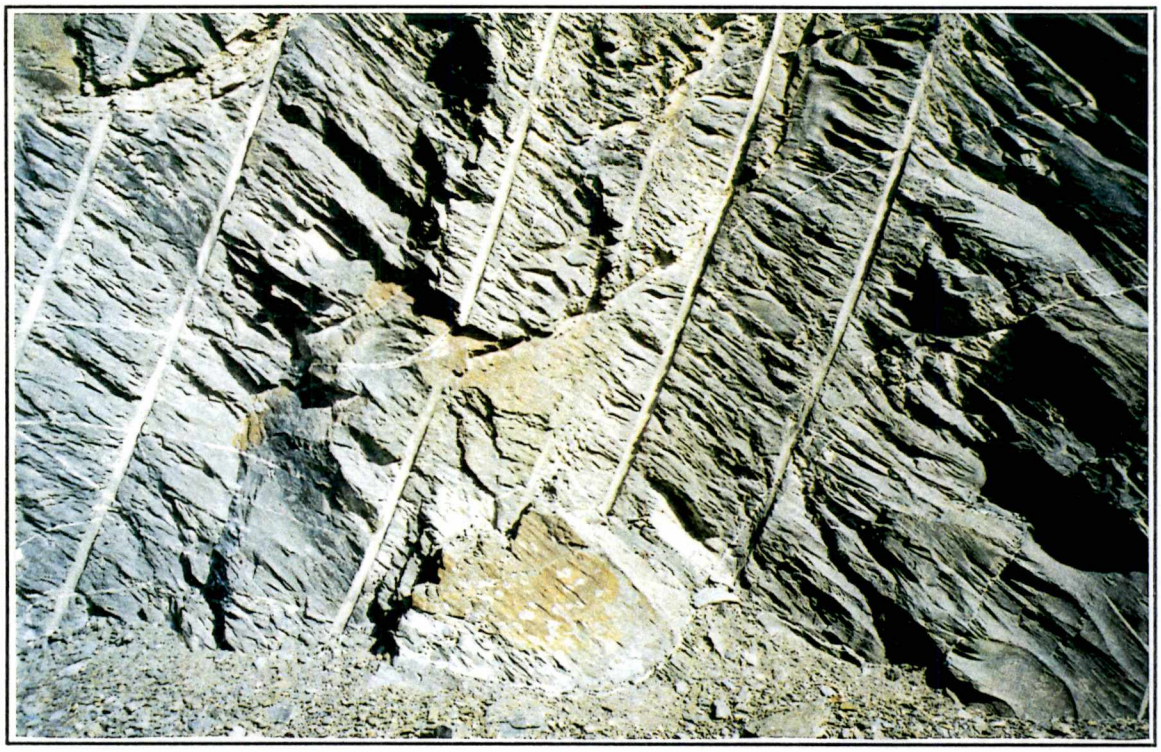


Figure 46 The folded bedding is shown by the quartzite cementation.



Figure 47 This block shows the thin bedding and perpendicular cleavage.

Field Data

The orientations of the planes measured at the Biltmore case study site are shown below in Table 3, with dip directions in degrees azimuth. Only the bedding planes and the bedding fractures were used in the calculation of the fold axis.

Table 3. Field data from the Biltmore site recorded December 1, 1995.

number	dip	dip direction	type
1	76	296	bedding fracture
2	77	311	bedding
3	78	326	bedding
4	74	303	bedding fracture
5	64	304	bedding
6	45	303	bedding
7	42	306	bedding
8	33	385	bedding
9	53	126	cleavage
10	78	309	bedding
11	81	319	bedding
12	82	302	bedding
13	86	308	bedding
14	85	314	bedding
15	81	308	bedding fracture
16	74	310	bedding
17	40	144	cleavage
18	63	170	cleavage
19	66	301	bedding
20	64	305	bedding fracture
21	59	306	bedding fracture
22	51	302	bedding
23	62	313	bedding fracture
24	61	311	bedding fracture
25	44	308	bedding fracture
26	35	307	bedding fracture
27	32	309	bedding fracture
28	28	307	bedding fracture
29	20	308	bedding fracture
30	18	306	bedding fracture
31	9	311	bedding fracture
32	11	313	bedding fracture
33	12	312	bedding fracture
34	46	132	cleavage
35	49	114	cleavage
36	43	314	bedding
37	55	316	bedding

38	46	313	bedding
39	46	311	bedding
40	36	334	bedding
41	29	324	bedding
42	10	397	bedding fracture
43	14	395	bedding fracture
44	8	231	bedding
45	6	233	bedding fracture
46	11	241	bedding fracture
47	8	235	bedding
48	4	239	bedding
49	10	234	bedding
50	78	109	cleavage
51	90	113	cleavage
52	8	204	bedding fracture
53	14	144	bedding fracture
54	16	136	bedding fracture
55	20	144	bedding
56	18	128	bedding
57	20	119	bedding
58	18	128	bedding
59	24	138	bedding fracture
60	23	139	bedding fracture
61	24	136	bedding fracture
62	30	140	bedding fracture
63	33	144	bedding fracture
64	34	148	bedding fracture
65	74	108	cleavage
66	76	124	cleavage
67	55	120	bedding
68	41	134	bedding
69	31	124	bedding
70	38	138	bedding
71	35	141	bedding
72	31	122	bedding
73	32	128	bedding
74	26	141	bedding
75	34	148	bedding
76	28	128	bedding
77	23	144	bedding
78	62	144	cleavage
79	51	143	cleavage
80	38	139	bedding
81	34	146	bedding

Figure 48 shows the approximate locations of the orientations taken on the slope. The bedding and cleavage is also outlined on the image.

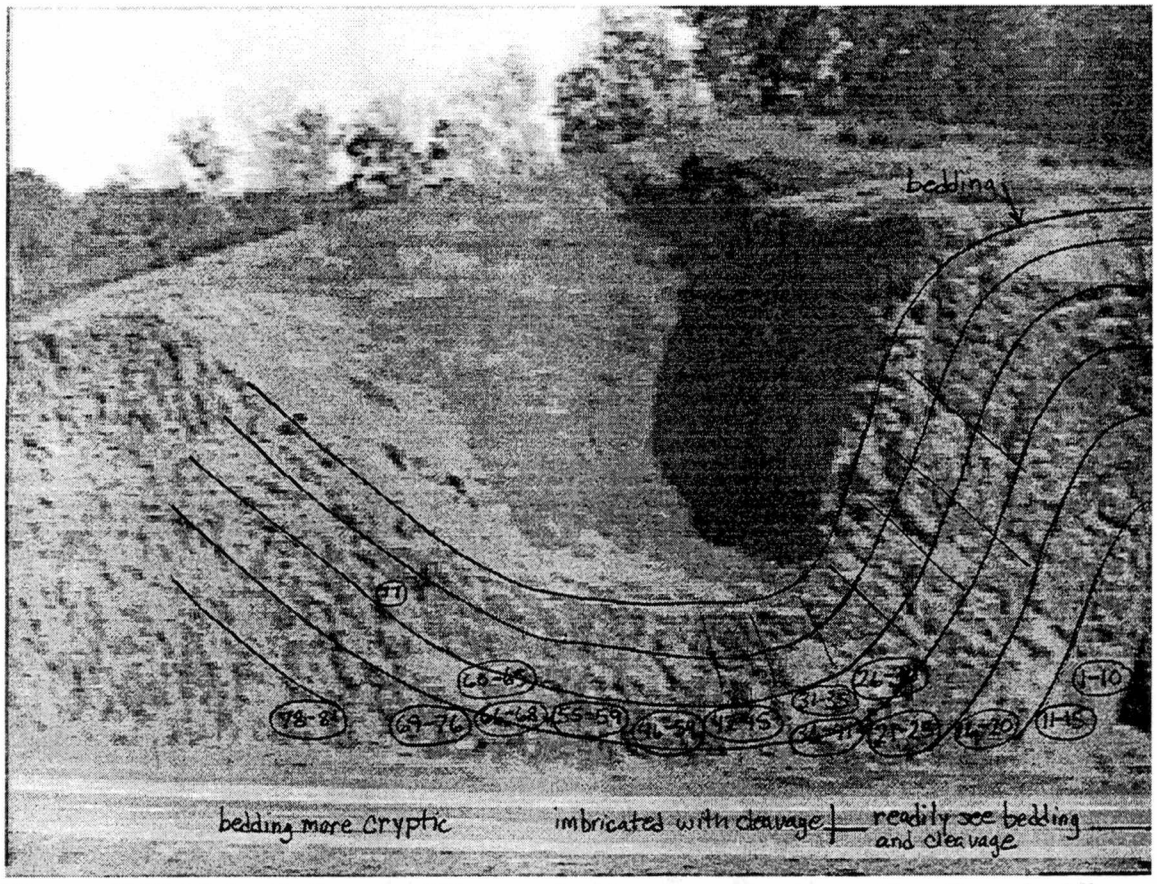


Figure 48 Field sketch from the Biltmore site showing measurement locations, bedding, and cleavage.

VITA

Scott Arwood grew up Lenoir City, Tennessee where he attended the public schools of Loudon County and Lenoir City. He graduated from Lenoir City High School in May 1990. He entered the University of Tennessee at Knoxville in August 1990 and received his Bachelors degree in Civil Engineering in 1994. He then entered graduate school at the University of Tennessee and served as a Graduate Research Assistant and Graduate Teaching Assistant within the Institute for Geotechnology, a research group within Department of Civil and Environmental Engineering. He received his Masters degree for this thesis project in August 1996.